University of Alberta

An Experimental Study of the Effect of Gravity and Electrostatic Field on Surface Tension and Contact Angles of Sessile Drops

by

Amjad Ahmad Ababneh

A thesis submitted to the Faculty of Graduate Studies and Research in partial fulfillment of the requirements for the degree of *Master of Science*

Department of *Mechanical Engineering*

Edmonton, Alberta
Spring, 2006

Your file Votre référence
ISBN: 0-494-13776-2
Our file Notre référence
ISBN: 0-494-13776-2

ABSTRACT

This thesis presents results of a series of experimental studies on the wetting of drops of pure liquids (water and hexadecane) on solid surfaces. The primary goal of these studies was to investigate the effects of body forces (gravity and electric field) on the surface tension and contact angles of liquid drops.

A suitable experimental setup that can be used on ground and in a reduced gravity environment was built for this purpose. Reduced gravity experiments were performed aboard a specially modified FALCON 20 business jet that flies a parabolic arc to produce short periods of reduced net acceleration force.

A difference of about 5° in the advancing contact angle was observed between the ground and the reduced gravity environment. Also, photographs of liquid drops in reduced gravity subjected to various electrostatic potentials were obtained that enabled the application of a novel methodology for determining the surface tension of liquids, Axisymmetric Drop Shape Analysis- Electric Field (ADSA-EF).

ACKNOWLEDGMENT

[58:11] "...Allah will raise up to (suitable) ranks (and degrees) those of you who believe and who have been granted knowledge".

The Holy Quran

I would like to thank God, Allah, for giving me the wisdom and knowledge, and helping me to finish this thesis work. It is He who guided me to talk to Dr. Elliott, in the beginning, and then Dr. Amifazli to supervise my study. It is He, in my opinion, who helped both my supervisors to receive the grant from Canadian Space Agency to do this thesis work.

I would like to thank both my supervisors; Dr. Amirfazli and Dr. Elliott for their guidance and support throughout this investigation.

I would like to thank my parents for their unlimited support. I would like to thank my brothers; Mazen, Mohammed, and Akram for their encouragement and patience.

I would like to thank Terry Nord and Dave Pape from the Mechanical Engineering Department for their help in setting up the electric circuit and machining of the apparatus.

I would like to thank my laboratory colleges (especially Colleen Chan and Javed Ally) for their help, advice, and support.

TABLE OF CONTENTS

LIST OF TABLES

LIST OF FIGURES

LIST OF SYMBOLS

P	Pressure
γ	Surface tension
R	Radius of curvature
ρ	Density
g	Gravitational acceleration
z	Vertical height
B_o	Bond number
a	Drop characteristic length
θ	Contact angle
R_c	Contact radius
h	Drop height
E	Energy
Q	Heat
t	Time

CHAPTER 1

INTRODUCTION

The physics of liquid/solid interfacial phenomena has been extensively studied before, including both experimental investigations and attempts to model and predict the shape of interfaces of liquid droplets on horizontal surfaces. Early speculation on the forces acting at the interface of two immiscible fluids began with the discovery of capillary phenomena by Leonardo da Vinci and later by Sir Isaac Newton[1]. However, Young[2] was the first to study this phenomenon both experimentally and theoretically.

> "Young established the theory of capillary phenomena by demonstrating how the principles of surface tension and contact angle can be used to explain a great many capillary phenomena. The theory was put on a firm mathematical foundation by Laplace[3]. Further developments were made by Gauss[4] who applied the principle of conservation of energy to the system and obtained not only the equation of the free surface but also the conditions of contact angle. Other earlier investigations include those by Rayleigh[5] and Gibbs[6] . Later investigations were carried out by Langmuir[7] and Harkins[8] in the U.S. and Adam[9] and Burdon[10] in England. Later on, surface phenomena were studied by many workers. Some of these investigations have concentrated primarily on contact angle, while others have devoted themselves to wetting and spreading"[11].

1.1. Interfacial Tension

1.1.1. An Overview

On a free liquid surface in contact with the atmosphere, there is little force attracting molecules away from the liquid because there are relatively few molecules in the vapor above the surface. Within the liquid bulk, the intermolecular forces of attraction and repulsion are balanced in all directions. However, for liquid molecules at the surface, the attractive forces of the next layer are not balanced by those in an identical layer above. This situation tends to pull the surface molecules tightly to the lower layer and to each other and causes the surface to behave as though it were a membrane in tension; hence, the name surface or interfacial tension. Surface tension has the unit of force per unit length or free energy per unit area.

The tension effects that occur on the surface of liquids, when the surfaces are in contact with another fluid or solid, depend fundamentally upon the relative sizes of intermolecular forces. Although such forces are negligible in many engineering problems, they may be predominant in cases such as; the capillary rise of liquids in narrow spaces, and the formation of liquid drops and air bubbles.

1.1.2. Interfacial Tension Measurements

Many techniques have been developed to measure interfacial tensions and detailed descriptions can be found in Adamson[12] and Neumann[13]. Some of these techniques are capillary rise, maximum bubble pressure, and capillary waves. Among all the methods which were developed, the Du Noűy ring[14] and the Wilhelmy plate[15] have been used most often; these methods measure the detachment force given by the surface tension multiplied by the periphery of the surface detached. Although both techniques are well

established and have been used primarily to measure liquid-vapor surface tensions, the Axisymmetric Drop Shape Analysis (ADSA) technique is a much more recent development and is attractive for measuring liquid-liquid interfacial tension as well.

1.2. Contact Angle

1.2.1. An Overview

When a liquid drop comes in contact with a flat solid surface, the angle measured within the liquid between the solid and the tangent to the liquid-gas interface at the three phase line is called the contact angle, θ. The key to understanding of the wettability of a liquid on a solid substrate surface is the recognition of the fact that it is determined by the balance of solid-liquid adhesive forces, which cause the drop to spread, and liquid-fluid adhesive forces, which cause the drop to bead up. Due to the interfacial forces, the liquid-solid system can be either completely wetting ($\theta = 0°$), partially wetting ($0° < \theta < 90°$) or non-wetting ($\theta > 90°$).

The study of wetting, adhesion and flotation requires knowledge of the contact angle. A liquid is wetting if it spreads easily across a surface. For example, insecticides should fully wet the surfaces of waxy leaves to protect the leaves from insects and disease. In the mining industry, flotation plays an important role in separating the minerals from the non-minerals in crushed ores. The mineral particles float to the surface by attachment to air bubbles. If the contact angle is finite, then the particle may be stably located at the interface.

Impurities present in, or added to, a liquid may alter the contact angle considerably. Wetting agents or detergents change the contact angle from a large value, greater than

90°, to a value often much smaller than 90°. Conversely, waterproofing agents applied to cloth cause the contact angle of water in contact with the cloth to be larger than 90°.

1.2.2. Contact Angle Measurement

Accurate measurement of contact angle is essential in many areas of applied surface thermodynamics. Direct measurement of contact angles from sessile drops is the most widely used technique. In this technique, the angle is measured by aligning a tangent with the drop profile at the point of contact with the solid surface. When first encountered, the measurement of contact angle appears to be quite straightforward. This apparent simplicity is however misleading and experience has shown that the acquisition of thermodynamically significant contact angles requires painstaking effort.

Many different techniques have been developed for the measurement of contact angles: Axisymmetric Drop Shape Analysis (ADSA), capillary rise, and the use of goniometer telescopes. ADSA is used to obtain the interfacial tension and the contact angle of a sessile or pendant drop and will be explained in more detail in the next section since it is the technique that has been used in this study.

1.3. Axisymmetric Drop Shape Analysis-Profile (ADSA-P)

The axisymmetric drop shape analysis-profile technique, as initiated by Rotenberg[16], is a user-oriented scheme to determine liquid-fluid interfacial tensions and contact angles from the shape of axisymmetric menisci, i.e., from sessile as well as pendant drops.

In essence, the shape of a drop is determined by a combination of surface tension and gravity effects. Small drops or bubbles will tend to be spherical because of surface forces. However, when gravitational and surface tension effects are comparable, then one can, in

principle, determine the surface tension from the measurements of the shape of the drop or bubble.

Both pendant and sessile drop methods require the solution of the Laplace equation of capillarity. The Laplace equation is the mechanical equilibrium condition for two homogeneous fluids separated by an interface. It relates the pressure difference across a curved interface to the surface tension and the curvature of the interface:

$$\Delta P = \gamma\left(\frac{1}{R_1}+\frac{1}{R_2}\right) \tag{1.1}$$

where ΔP is the pressure difference across the interface, γ is the interfacial tension, and R_1 and R_2 are the principal radii of curvature. In the absence of any external forces other than gravity and for sufficiently small elevation changes, ΔP may be expressed as a linear function of the elevation:

$$\Delta P = \Delta P_0 + (\Delta\rho)gz \tag{1.2}$$

where ΔP_0 is the pressure difference across the interface at the reference plane, $\Delta\rho$ is the density difference between the two bulk phases, g is the gravitational acceleration, and z is the vertical height measured from the reference plane.

1.4. Definition of Reduced Gravity

> "The term "zero gravity" or "micro gravity" is a misnomer even though these terms have been used extensively in literature. Even on the most advanced interplanetary mission, gravitational forces are never totally absent. A reduced gravity (micro gravity or zero gravity) environment refers to those situations

where the statics or dynamics of a system relative to its traveling vehicle can be treated as a reduced gravity field.

The term zero-g or microgravity must be interpreted to mean that the difference between the local acceleration of the particle in the gravitational field (g) and the vehicle acceleration (a) is sufficiently small that the effect of body forces seen by an observer moving in the reference frame of the vehicle are very small compared to the other forces, and consequently do not influence the behavior of the fluid drops"[11].

1.5. Objective of the Present Thesis

Liquid behavior in reduced gravity under static and dynamic conditions is markedly different than in normal earth gravity. In general, the forces acting on a liquid drop are inertial forces (due to gravity) and intermolecular forces between liquid molecules (cohesion) and between liquid molecules and solid surfaces (adhesion). These intermolecular forces are exhibited in the form of surface tension forces.

The Bond number, B_o, has been introduced as the ratio of the effects of the gravitational forces to the effects of surface tension forces, that is

$$B_o = \frac{\rho g a^2}{\gamma}$$

where ρ is the liquid density, g is gravitational acceleration, a is the drop characteristic length, and γ is the liquid surface tension. When a liquid drop is under the effect of a gravitational field, the inertial forces predominate if the Bond number is much greater than unity and only small effects of surface tension forces are noticeable. Typically, the effects of dominant inertial forces shape the liquid drop. When a liquid drop is removed from the effects of a gravitational field however, the surface tension forces become significant because the inertial forces are no longer dominant. The present work is

concerned primarily with wetting systems where the relative importance of body forces and capillary forces on liquid drops is varied.

The present thesis is focused on the following two areas:

1. The effect of electric field on surface tension of sessile liquid drops in the absence of a gravitational field.
2. The effect of gravity on the advancing contact angle of sessile drops.

The behavior of liquid drops and bubbles in electric fields and in the absence of gravity is of fundamental importance in developing existing and new technologies on ground and in space, e.g., electrostatic spraying, ink jet printing, physical and chemical separation, and alloy research in space. Two of the key properties in determining the behavior of drops are surface tension and contact angle. The effect of electric field on surface tension of liquid drops as well as the effect of gravity on the advancing contact angle are not understood well at the present time mainly due to the absence of a suitable methodology. It is expected that findings will generate the necessary data that should allow better understanding regarding the effect of electric field and gravity on surface tension and contact angle.

The importance of establishing a proper advancing contact angle cannot be overemphasized since, on properly prepared solid surfaces, this is the only contact angle which is unique and has thermodynamic significance. The effect of gravity on the advancing contact angles of sessile drops is not clear due to the lack of a suitable methodology to study this effect in a reduced gravity environment.

1.6. Scope of the Thesis

In the first phase of this study, a suitable experimental apparatus was built to allow experimentation for two separate studies: the effect of the electric field on surface tension of liquids in reduced gravity conditions as well as the study of the effect of gravity on the advancing contact angle of sessile drops. The second phase of this study was to conduct the experiments in a reduced gravity environment and on the ground. In each experiment, a drop was produced atop a Teflon-coated silicon wafer and its image was digitally recorded for subsequent analysis. The third phase of this study was to analyze the advancing contact angle experiment images acquired in the reduced gravity and on the ground and to compare the results of the different environments with each other.

CHAPTER 2

EXPERIMENTAL SETUP

The same setup was used for the ground-based and the reduced gravity experiments. Test equipment intended for use on reduced gravity flights must conform to special requirements. The entire equipment should be fixed down; no loose or free floating items are allowed; all exposed edges and corners should be padded; and cables should be tied or taped down. In order to minimize motion sickness of the operator the experimental setup should be designed to minimize the operator's head movements during the flight. Extensive head motions during zero-g can provoke motion sickness. Any tools required should be attached to the experimental apparatus with Velcro or duct tape.

The test setup (Fig. 2.1) is composed of the following components: frame, test cell, CCD camera, camcorder, main power supply, high-voltage power supply, lighting, diffuser glass, and laptop computer.

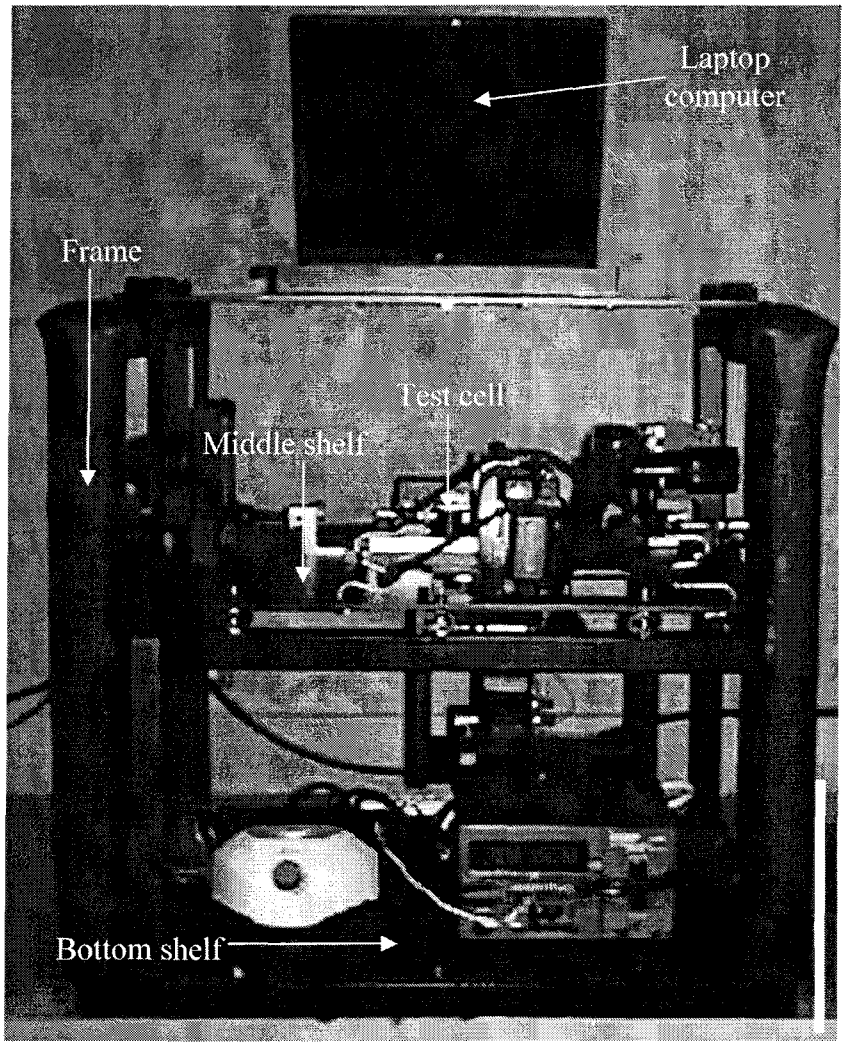

Figure 2.1 The experimental setup

All the components were mounted on three shelves on the frame. The shelves were painted black to minimize the effect of light reflection on the drop. The top shelf was used to mount a laptop-computer. The middle shelf (Fig. 2.2) was used to mount the main components of the experiment, which include the test cell, camcorder, CCD camera, lighting and frosted glass. The bottom shelf was used to mount other experimental

support components, such as power supplies for the motor drive and light source, the stepper-motor drive, camcorder battery, and power bar.

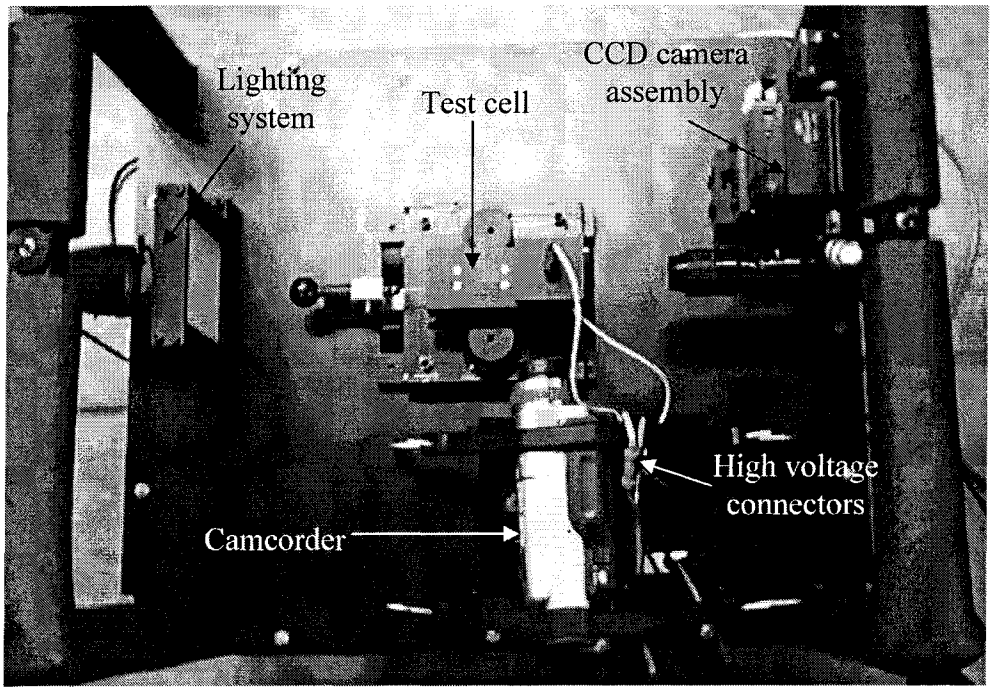

Figure 2.2 Top view of the middle shelf of the experimental setup

The test cell is the main component of the experimental setup. It contains two electric field disks and a syringe. The main power supply was used to run and control the stepper-motor which was used to push the plunger of the syringe to generate the drop. It was also used as a power input to the high voltage power supply which was used to apply electric field on the drop through the electric field disks. The CCD camera was used to take images of the drop as viewed along the fore-aft axis of the plane which were used for analysis. The mounting of the CCD camera was chosen along the fore-aft axis because the vibration on the lateral axis is less than the vibration along the fore-aft axis. The camcorder was used to take side-view videos of the drop to observe the effect of the

vibration on the images. The camcorder was also used to make audio comments during the flights. The laptop computer was used to run the image acquisition program necessary for the CCD camera and the motor-drive program to run the motor to generate the drops.

2.1. Frame

The frame (Fig. 2.3) was designed by R. Chiang to fit the "single mounting" rack as shown in the *Falcon 20 User's Guide*[17] while supporting and protecting all the equipment that is required for the experiment. The frame was covered with pipe insulation (Fig. 2.1) for the safety of the operator.

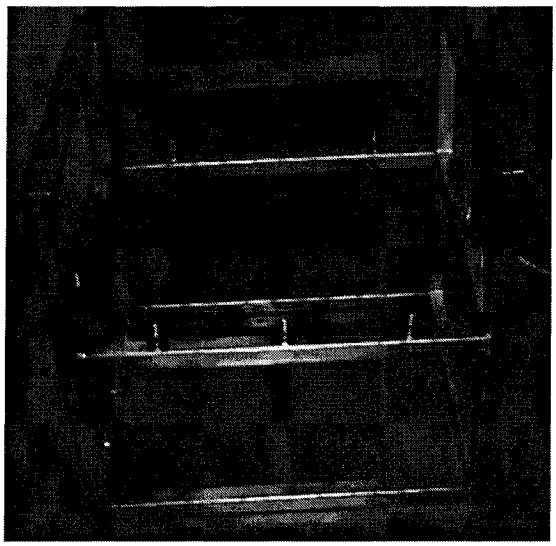

Figure 2.3 The frame

The frame, as shown in Fig. 2.3., was constructed previously from 1010 mild steel square profile with dimensions of 1.25" (3.175 cm) and a wall thickness of 1/16" (0.15875 cm). The steel profiles are TIG welded into a rectangular frame. The frame weighs approximately 25 pounds (11.34 kg). The frame was modified to support three

shelves (Fig. 2.1) made of 1/4" (0.635 cm) aluminum plates. The middle (main) shelf was mounted on vibration isolators to reduce the effect of vibration caused by the plane.

2.2. Test Cell

A typical flight consists of four parabolas. Each of these parabolas is separated by about three minutes or, if required, enough time to alter the test setup. Therefore, four similar test cells were manufactured and used in the experiment. The design of the test cell incorporates a number of features which make it easy to use, reliable and accurate. For easy removal and replacement of the test cell, the test cell was connected to the high voltage power supply through high voltage wires and connectors (Caton connector corp., series 14). Also, two rotary clamps were mounted on the sides of the test cell and used to hold down the test cell. Also, a rotary plunger holder is used to hold and push the syringe-plunger. Two pins in the test cell plate were added for mating two holes in the bottom of the test cell. In addition to these features, the test cell should have the capability to function in two different experiments, i.e., the electric field experiment and the advancing contact angle experiment. Pro/Engineer®, a Computer-Aided Design package developed by Parametric Technologies Corporation (PTC), was used in the design of the test cell (Fig. 2.4).

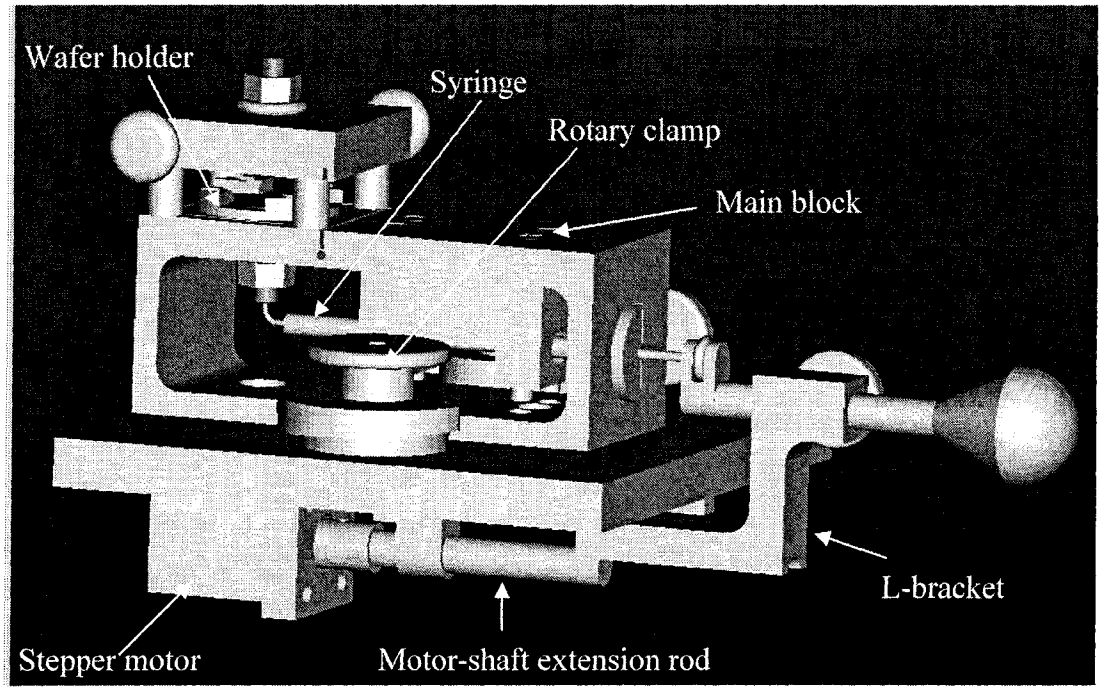

Figure 2.4 CAD drawing of the test cell assembly

The stepper motor (NEMA 11 Step Motor, Applied Motion Products, Inc.), which was mounted underneath the test cell, pushes a linear slide through a motor-shaft attachment rod (Fig. 2.5).

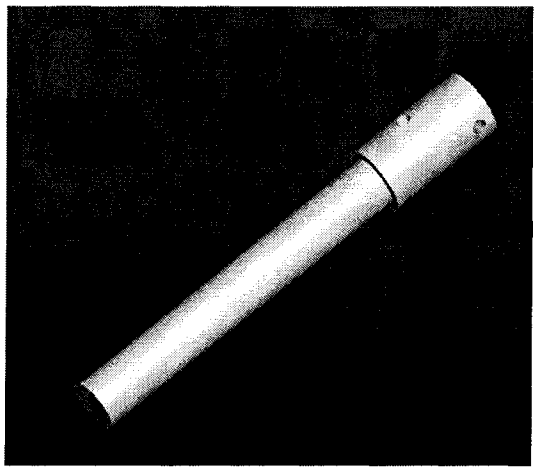

Figure 2.5 Motor-shaft extension rod

The linear slide is attached to an L-shape bracket, which pushes in turn the plunger of the syringe. The tip of the syringe needle was flush with the silicon substrate where the drop was to be formed. The body of the test cell was made of black Delrin. Black Delrin was chosen for its mechanical properties such as high strength and rigidity over a broad temperature range, toughness and good electrical insulation. The color black was used to eliminate reflections of light from the material, which might interfere with the measurements.

The main block (Fig. 2.6) is a rectangular block that forms the main body of the test cell.

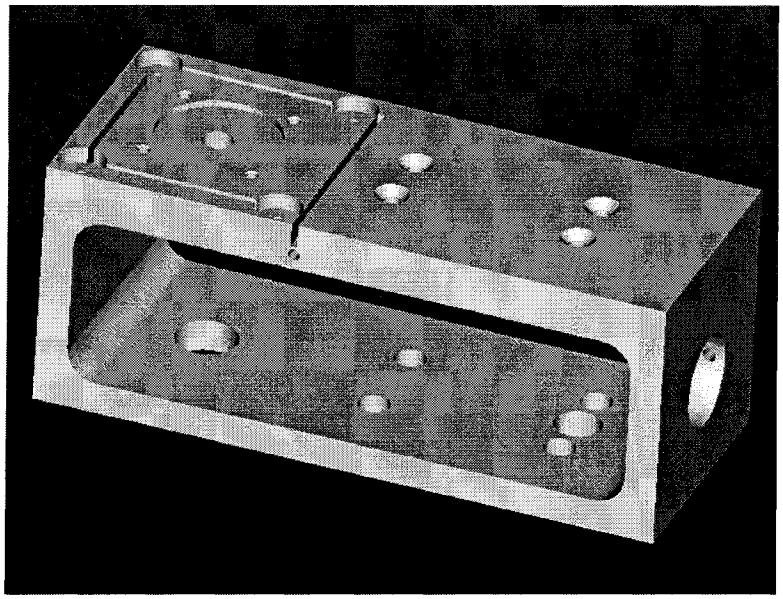

Figure 2.6 Test cell main block

The main block holds the syringe and the electric field disks by means of electric field disk supporters (Fig. 2.7). For easily removing and replacing the test cells during the flight, the operating test cell was mounted on the apparatus by two rotary clamps (Fig. 2.8).

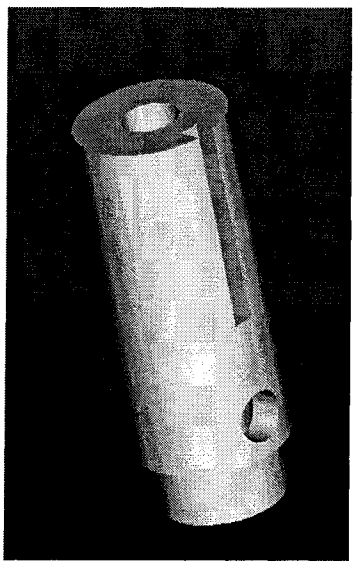

Figure 2.7 Electric field disk support

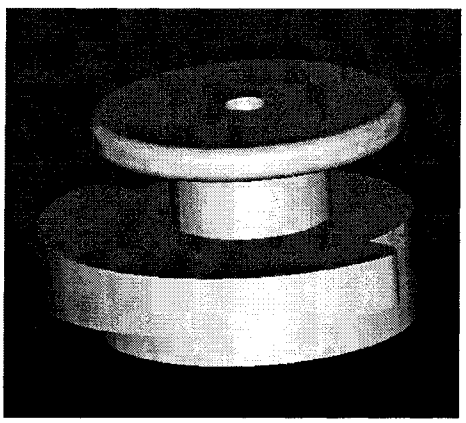

Figure 2.8 Rotary clamp used on both sides of the test cell to mount the test cell to the test cell plate

The main block has two holes on the bottom side to match two pins on the test cell base plate (Fig. 2.9) for easy mounting and alignment. The base plate is made of aluminum and provides support and rigidity to the test cell. It is fastened to the main shelf

by four screws, one on each corner. The stepper motor was mounted on a motor-holder (Fig. 2.10) underneath the test cell plate.

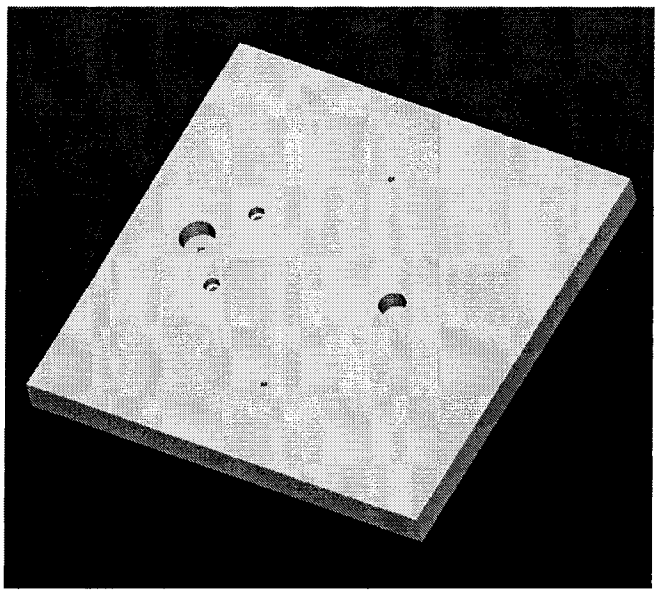

Figure 2.9 Test cell base plate

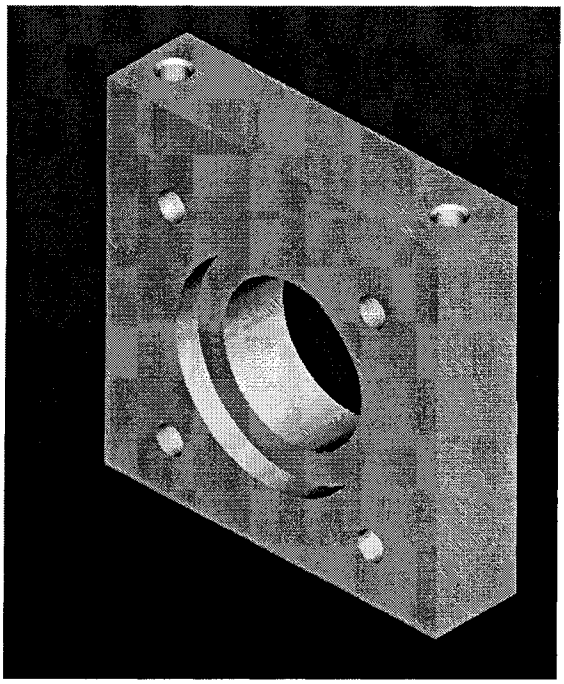

Figure 2.10 Motor holder

A programmable stepper drive, model 1240i (Applied Motion Products, Inc.), was mounted on the bottom shelf. The motor-drive includes software (Applied Motion's Si Programmer Windows) that was installed in the laptop computer to control the drop formation and advancing by controlling the motor operation.

Two electric field disks (Fig. 2.11) were made of copper since it is easily machined and has good electrical conductivity.

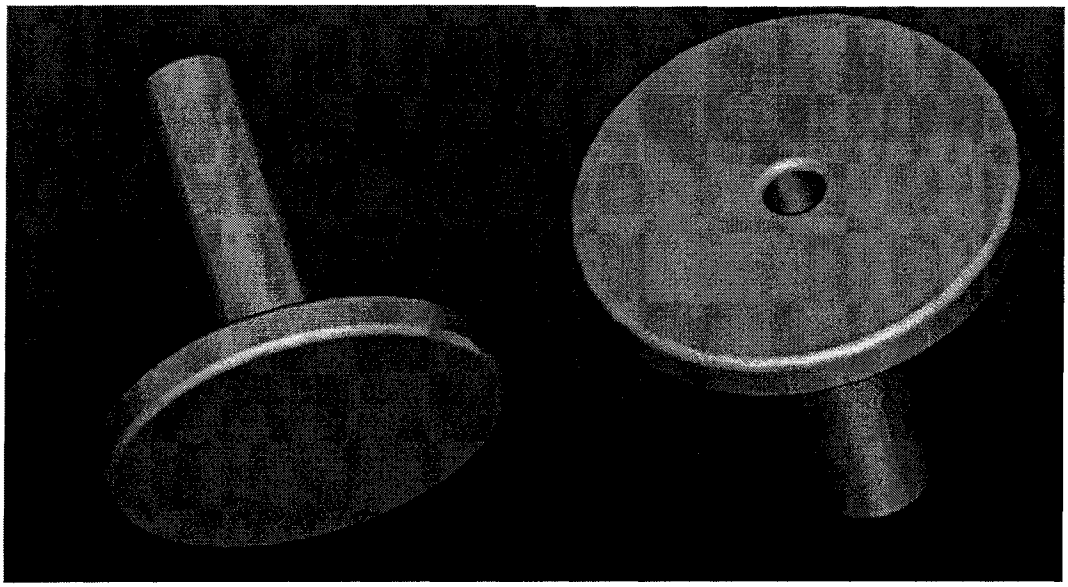

Fig. 2.11 Upper (left) and lower (right) electric field disks

These two copper disks were used as capacitor plates to apply electric field on the drop. To change the distance between the disks as needed, a threaded rod protrudes from each disk, which by rotating moves up or down. The lower disk has a through-hole to allow the insertion of the needle. All edges of the disks were rounded to reduce arcing and distortions of the electric field. These disks sit on the top of the base block and are separated by four circular columns made of Delrin. Glass slides were to encase the disks and droplet to minimize the effects of evaporation or air currents during the experiments. They were also used to isolate the field disks for the safety of the operator. The silicon wafer was mounted on the top of the lower electric field disk by a wafer holder (Fig. 2.12). Complete drawings of the test cell with dimensions can be found in Appendix-A.

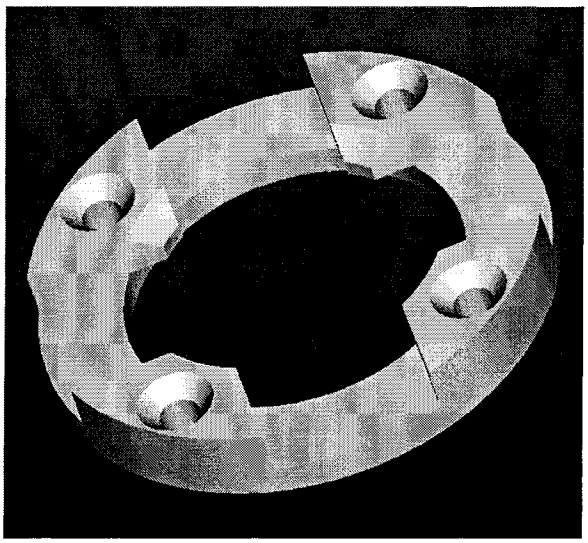

Figure 2.12 Wafer holder

2.3. CCD camera

A CCD camera (PixeLINK PL-A662) was used to record the images of the drop as viewed from the direction of the fore-aft axis of the aircraft. The reason for choosing this direction is because it is believed that the airplane vibration is minimal in this direction. The images of the drop were taken before, during and after the reduced gravity by using a special program installed in the laptop computer. Only images taken during the reduced gravity period were used for analysis.

A ball bearing linear stage (NEWPORT M423 series) was used to mount the CCD camera and the lens to control precisely the position of the camera. These mounts are necessary to adjust the vertical and horizontal position of the camera and make sure that it is aimed at the drop during the experiment.

2.4. Camcorder

A digital video camera (Sony DCR-TRV 530) was used to record the lateral view of the drop. The camcorder accepts both DC (battery) and AC power sources. For the experiment, an AC adaptor was used to power the camera. The camcorder is strapped down using stretch cords to mitigate any vibration problems that might arise due to the camcorder mounts.

2.5. CCD Camera Lens

For compact design, right angle attachment (NAVITAR, 1-6080) was used, introducing a 90° bend in the optical axis, shortening the overall length of the system. The resulting image was mirrored and read side up down when viewed with the camera. To avoid this unwanted consequence, the camera was rotated 180° to produce an image of the drop as physically situated. An additional lens attachment (x16) was used in the electric field experiments to magnify the drop image.

2.6. Lighting

A halogen lamp (Licia Model 13410311) was used to illuminate the drop from behind. The lamp was mounted on an aluminum post whereas the light control box was mounted on the bottom shelf. No lighting was needed for the camcorder since the night shot recording option was used.

2.7. Diffuser Glass

The diffuser glass was necessary to diffuse the back light of the drop to produce a uniform background for the drop images. The frame of the glass was built from

aluminum and was mounted in front of the lighting. The frame was also painted in black to minimize the effect of light reflection.

2.8. Power Supply

A digital triple output DC power supply (Extech Instruments, 382213 model) was used to supply the necessary power to run the stepper motor. This power supply has three adjustable outputs: 30V/3A and fixed 5V and 12V outputs. The 12V fixed output was used to run the stepper motor while the 5V output was used to control the operation of the stepper motor by using an electrical switch. The variable output of the power supply was used as an input to the high voltage power supply which was used to apply electric field across the drop in the electric field experiments. The variable output was not used in the advancing contact angle experiments since it was not needed.

2.9. High Voltage Power Supply

An EMCO (E101) high voltage power converter was used to provide the high voltage needed between the plates of the capacitor as shown in Figure 2.13. A triple output power supply was used to provide power to the stepper motor drive and the voltage required to operate the high voltage power converter. High voltage power connectors and wires (Caton Connector Corp., 14 series) were used to transfer the power between the high voltage power supply and the electric field disks.

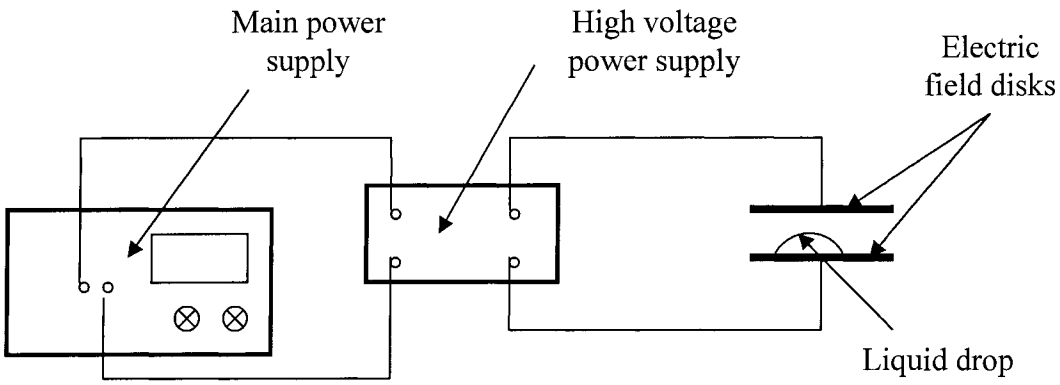

Figure 2.13 Schematic of the electric circuit for drop charging

2.10. Laptop-Computer

The laptop computer was necessary in this experiment for two reasons. Firstly, it was needed to run the program needed to operate the drop generation mechanism (linear slide, plunger handle, and syringe). Secondly, it was also necessary to capture and monitor drop images taken by the CCD camera.

CHAPTER 3

GROUND AND REDUCED GRAVITY EXPERIMENTS

3.1. Objective and Description of the Experiments

3.1.1. Electric Field Experiments

Electric field experiments were planned for the determination of the effect of electric field on surface tension using polar and non-polar liquids (i.e. water and hexadecane). In this experiment, a droplet was formed within the parallel plate capacitor and its images were digitally recorded for subsequent analysis on the ground. The drops formed were of 2-3 mm in base diameter on Teflon-coated silicon wafers subject to a variable potential ranging from 0 to 10 kV in reduced gravity. Two different water drop sizes were studied; 2 and 4 $\mu\ell$ whereas hexadecane droplets were limited to one size only because it was expected not to see any effect of the electric field on the hexadecane due to the non-polarity of the hexadecane. For each case in reduced gravity three experimental runs were achieved to gauge the reproducibility of data. The images of the reduced gravity experiments were used by another student, Arash Bateni, for the determination of the effect of electric field on surface tension[18].

3.1.2. Advancing Contact Angle Experiments

Advancing contact angle experiments were planned for determination of the effect of gravity on the advancing contact angle using only purified water. In this experiment, a drop was formed atop a Teflon-coated silicon wafer and the contact line was continuously advanced while images of the drop were digitally recorded during the

advancing period for subsequent analysis. A similar procedure was followed for the ground and reduced gravity environments to compare the effect of gravity on the advancing contact angle.

3.2. Materials Used

3.2.1. Solid Surfaces

Silicon wafers (Type N, 1" diameter, orient 100, 250-350 μm thickness) were purchased from Wafer World, Inc., FL. The 1-inch silicon wafers were used in the reduced gravity experiments. Because of the high cost of the 1-inch, type N silicon wafers, a different size and type of silicon wafers (Type P/Boron, 100 mm diameter, orient 100, 415-456 μm thickness) were purchased from Nanofab, University of Alberta and used in some of the advancing contact angle ground-based experiments.

3.2.2. Liquids

A 6% solution of Teflon AF 1600 resin, purchased from Dupont Co., was selected as the coating material. Purified water (Millipore Direct-Q) was used as the test liquid (18.2 $M\Omega.cm$ at 25 $^{\circ}C$). Hexadecane was also used in the electric field experiment.

3.3. Experimental Procedure

3.3.1. Wafer Cleaning and Coating Procedures

The cleaning and coating procedures for both kinds of wafers were the same. A hole of approximately 1 mm in diameter was drilled in the center of each surface by means a diamond drill bit (UKAM Industrial superhard tools, CA). In order to obtain smooth coated films, the 6% Teflon solution was diluted with FC-75 at a 1/3 volumetric ratio.

The surfaces were coated by a dip-coating technique as follows: The wafer surfaces were put in a sonicator (Elma, transonic 460) for about 10 minutes, rinsed with acetone and washed again with distilled water. They were then soaked in chromic acid (Fisher Scientific) for at least 24 hours and subsequently rinsed with distilled water. The cleaned substrates were left under a heat lamp to dry. The cleaned surfaces were immersed vertically into the coating solution at a speed of c.a. 7×10^{-2} *cm/s* and withdrawn at the same speed. Finally, the coated wafers were left in a vacuum oven at a temperature of 165 *°C* for 3-5 hours. For the reduced gravity experiment, the wafers were packed in air-tight cell-holders to transport them to the flight site.

3.3.2. Reduced Gravity Experiments

The reduced gravity environment was produced with a specially modified FALCON 20 business jet (provided by the National Research Council, Flight Research Laboratory, through an agreement with the Canadian Space Agency) that flies a parabolic arc to produce short periods of reduced net acceleration force. In total, 12 parabolas have been carried out for the advancing contact angle experiment whereas 36 parabolas have been carried out for the electric field experiment. Due to the extraordinary circumstances of the flight environment, the number of successful parabolas for each experiment was 9 for the advancing contact angle and 27 for the electric field experiment.

Four parabolas per flight were typically achieved with a reduced gravity period lasting about 20 seconds. During most of the reduced gravity portion, the g-level produced was slightly positive but under 0.01g (Fig. 3.1). The low-g period was preceded and followed by short ~2g periods (called pull-up and pull-out).

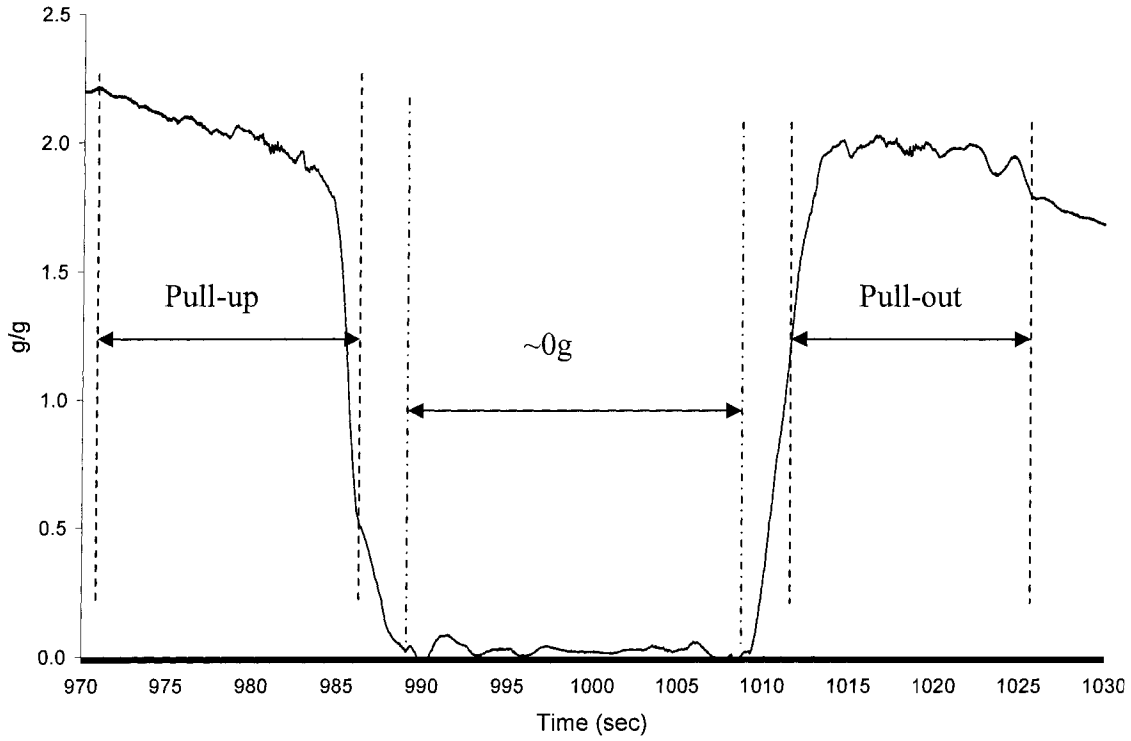

Figure 3.1 Typical reduced gravity conditions

Three flight campaigns were launched. The first campaign was scheduled in March, 2004 but it was delayed to May, 2004 due to scheduling arrangements by CSA. The first campaign was used solely for the electric field experiments. The other two campaigns were launched in July and September of the same year. One operator was required to conduct the reduced gravity experiments. A second operator was necessary for the first campaign to help with the experimental procedure so that the first operator could get used to the reduced gravity environment. The second operator was also helpful in the electric field experiment since the procedure involves more than one step happening at the same time. Also, the second operator was necessary in case the principal operator experienced motion sickness.

Several tasks were performed prior to, during, and after the flight. A checklist was developed and checked before the flight (Appendix-B) after the experimental setup was installed onboard the aircraft.

For the electric field experiments, the procedure started approximately 10 seconds before entering reduced gravity by generating the drop by running the stepper motor drive. Then the drop was advanced and the electric field was gradually increased to the desired level for each parabola by increasing the variable voltage of the main power supply upon entering the reduced gravity environment. The program for generating and advancing the drop is shown below. Step 2 in the program is the generation of the drop whereas step 4 is for advancing the drop. Table 3.1 shows the timing and sequence of events in a typical run for the electric field experiment.

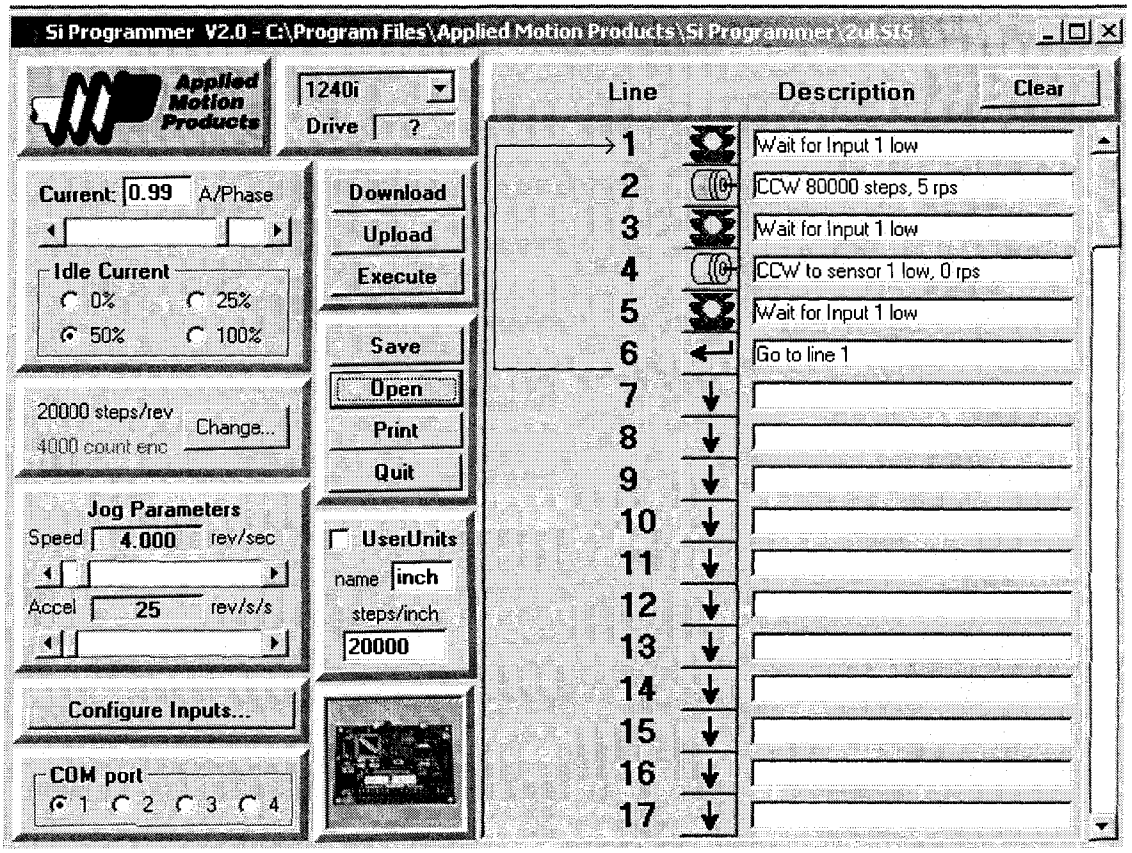

Figure 3.2 Graphical user interface (GUI) for stepper-motor program for the electric field experiments

The procedure for the advancing contact angle experiments was slightly different. No electric field was applied in these experiments and the advancement of the drop took place for the whole period of reduced gravity. To keep the contact line advancing rate constant, two different pumping rates were used. Figure 3.3 shows the program for generating and advancing the drop. Step 4 in the program represents the generation of the drop whereas steps 6, 7, and 8 are used to advance the drop at faster advancing rates subsequently.

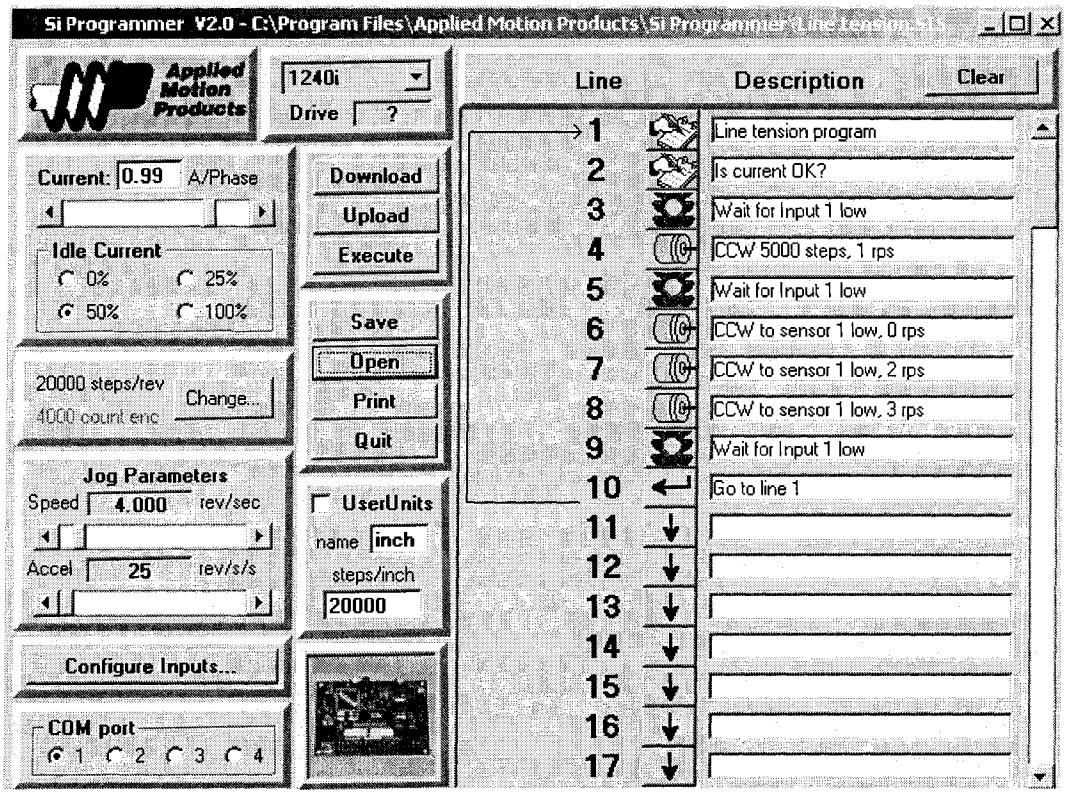

Figure 3.3 Graphical user interface (GUI) for stepper motor program for the advancing contact angle experiments

Since the final drop size is much bigger than the drop size in the electric field experiment, a lens attachment was used to fit the drop size in the view field of the CCD camera.

After the reduced gravity and between parabolas, the test cell was replaced with a new one by turning off the main power supply and disconnecting the high voltage power connectors for the electric field experiments. The used test cell was then removed by releasing the main block by rotating the rotary clamps and the plunger clamp. A new cell was mounted in the same place by virtue of the two rotary clamps on the side of the cell and two holes in the bottom of the main block that match two pins on the test plate.

After each flight, the images were checked for any malfunction of the CCD camera and also to back up the images to a USB drive.

3.3.3. Ground Experiments

The ground experimental procedure was much simpler than the reduced gravity procedure since there is no need to worry about loose or floating items. The ground experiments were conducted at the University of Alberta by using the same experimental setup and the same stepper-motor program that were used in the microgravity flights. Several contact line advancing rates were studied to investigate the effect of the contact line advancing rate on the advancing contact angle for the advancing contact angle experiment. For the electric field experiments, the images were sent to Arash Bateni at the University of Toronto for further analysis.

Table 3.1 Timing and sequence of events in a typical run for the electric field experiment

Gravity	Present	Microgravity										Present
Time (s)		1	2	3	4	5	6 ...16	17	18	19	20	
Drop generation	-10 - 0											
Drop advancing												
Field ramp-up												
Field level steady												
Camera on	-20											+40
Light on	-20											+40
Temp. recording	-20											+40
2nd Field ramp-up*												
Field ramp-down												+ 23
Field off												+23 →
G recording	-20											+30
Drop disposal												+23→ 40

* Except the last run in a set of experiments for a particular condition, this step will not take place; the field strength will remain the same.

CHAPTER 4

EFFECT OF GRAVITY ON THE MACROSCOPIC ADVANCING CONTACT ANGLE OF SESSILE DROPS

4.1. Introduction

The contact angle of a sessile drop, i.e., the angle formed by the free surface of the drop with the solid substrate, is governed by mechanical equilibrium under the action of three interfacial tensions: liquid–vapor γ_{lv}, solid–vapor γ_{sv}, and solid–liquid γ_{sl} surface tensions. The three interfacial tensions and the contact angle are related by Young's equation:

$$\gamma_{lv} \cos\theta_Y = \gamma_{sv} - \gamma_{sl} \tag{4.1}$$

Equation (4.1) stipulates a single, unique contact angle for a liquid droplet placed on an ideal solid surface (i.e., homogeneous, planar and smooth) corresponding to thermodynamic equilibrium. This contact angle, which can be called the macroscopic contact angle, is used as the boundary condition for the macroscopic hydrodynamic equation in flow fields and for the Laplace equation to determine the surface shape. However, the experimentally observed macroscopic, static contact angle, θ_s, may or may not be the Young contact angle, θ_Y.

With increasing volume of the drop and hence the contact radius, one can ensure that the contact angle of the drop reaches a reproducible advancing contact angle, which has been assumed to be meaningful in terms of Young's equation for low-rate advancing

contact lines. It is important to realize that even though static contact angles are reported, they may be erroneous and many careful experiments deduce its value from dynamic measurements.[19,20]

The advancing contact angle, i.e., the angle formed by the free surface with the solid substrate when the three-phase contact line is advancing (Fig. 4.1), is important in many natural and industrial processes, e.g., coating of solids by liquid films, tertiary oil recovery, mineral processing, spraying of pesticides, and textile manufacturing. For example, Wege et al.[21] showed that dynamic contact angle and spreading rate measurements can be used for the characterization of the effect of dentin surface treatment on adhesion of restorative materials to dental tissues. Ngan and Dussan[22] showed that, in contrast to static wetting, the measurement of a dynamic contact angle near the contact line strongly depends on the macroscopic scale. Therefore, such measurements made in one geometry may not necessarily be used to predict the dynamics in another geometry. Blake and Shikhmurzaev[23] also mentioned that the dynamic contact angle depends not just on the contact-line advancing rate but also on the entire flow field in the vicinity of the moving contact line.

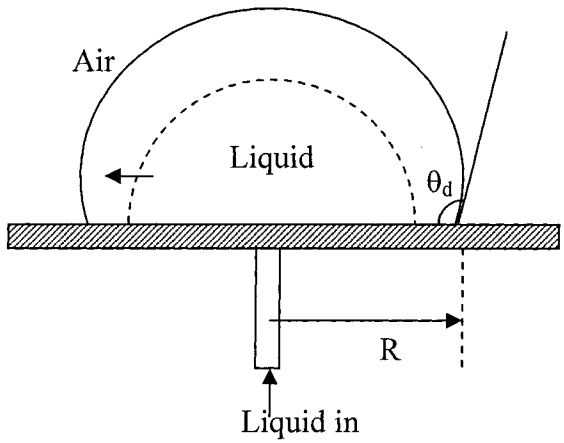

Figure 4.1 Schematic diagram of hydrodynamically forced spreading of a sessile drop on a solid surface

A few detailed observations of the effect of gravity on the macroscopic contact angle have been reported in the literature. Ward et al.[24] and Sasges and Ward[25] conducted experiments on a space shuttle flight and on ground to study a closed, two-phase capillary system (with a liquid phase both above and below a vapor phase). They showed that the static contact angle at the upper three-phase line is smaller than that at the lower three-phase line and explained this phenomenon as being due to the gravity induced pressure difference between the liquid phases of the two-interface configuration. The results were in a good agreement with their theoretical thermodynamic analysis based on the Gibbs model of the interface and the resulting necessary conditions for equilibrium[26] and showed that the difference they observed between the upper and lower contact angles is a result of pressure variation with elevation. Abel et al.[27] measured the contact angles of a drop expanded and withdrawn atop another immiscible liquid in the reduced gravity environment of parabolic flights. They observed a considerable contact angle hysteresis

where it should not have existed as liquid-liquid-fluid systems generally do not exhibit a considerable contact angle hysteresis. Judging by the estimated capillary number ($Ca \approx 0.02$); they pointed out viscosity effects as a possible cause of the observed contact angle hysteresis. Dreyer et al.[28] studied the liquid flow between parallel plates due to capillary rise under reduced gravity. Experiments were performed during free fall in a drop tower to investigate the transient rise of the meniscus (free surface). They used a perfectly wetting fluid (zero degree static contact angle) and neglected any dynamic contact angle effects.

Another issue of concern in the study of sessile drop advancing contact angles is the effect of liquid pumping rate, and hence the three-phase contact-line advancing rate, on the advancing contact angle. Kwok et al.[29] studied sessile drops of 17 different liquids, including water, on FC-722 dip-coated mica surfaces, with contact angles ranging from 66° to 118°. They showed that the low-rate (less than 0.52 mm/min advancing rate) dynamic contact angles in 1g for a sessile drop were essentially independent of the velocity of the three-phase contact line and identical to the static advancing angles. However, it is unclear whether the rate independence for contact angles will hold under reduced gravity conditions where the hydrodynamics are different. This is especially important as Blake and Shikhmurzaev[30] have shown that a considerable change in viscosity (e.g. by one or two orders of magnitude) can result in a different contact angle due mainly to different hydrodynamics at the three-phase line.

In this thesis, we present our findings for advancing contact angles measured for a sessile drop on a solid surface in reduced gravity and compare them to results from an identical system on the ground.

4.2. Contact Angle Measurements

Calculation of the contact angle from the digitized images was accomplished by the axisymmetric drop shape analysis-profile (ADSA-P) technique. To take advantage of the very nearly spherical shape of the drop in the reduced gravity environment; geometrical relations for a spherical cap were also used to calculate the contact angle, θ:

$$\theta = \frac{\pi}{2} + \cos^{-1}\left(\frac{2R_c h}{R_c^{\,2} + h^2}\right) \tag{4.2}$$

where R_c is the contact radius and h is the height of the drop. The contact radius and the height of the drop were found by superimposing the image of a calibration grid on the image of the drop (Fig. 4.2). The results for both methods were found to be in a good agreement with each other for the images of reduced gravity.

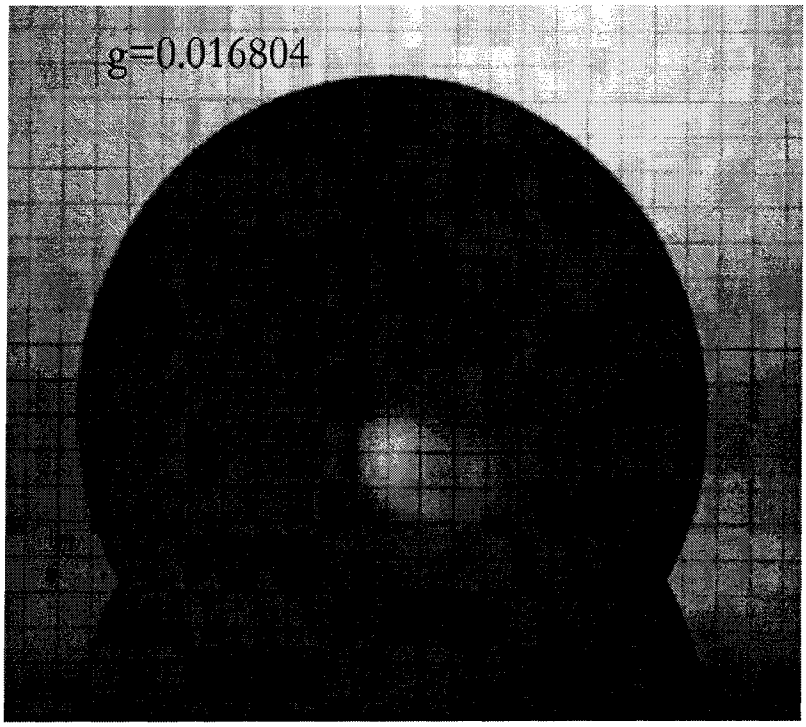

Figure 4.2 Superimposed image of the grid on a drop image in reduced gravity

4.3. Results and Discussion

The effect of the liquid pumping rate, and hence the three-phase contact line advancing-rate, on the advancing contact angle was studied in 1g. The results were analyzed using ADSA-P and the advancing rates were obtained from the slope of the contact radius with time as shown in Fig. 4.3. The regression coefficient for the contact radius versus time (image number) was found to be 0.99; this indicates that the rate of change of the three-phase contact line can be approximated as constant for the pumping rates used in the experiment, even though it was controlled only by manipulating the drop volume.

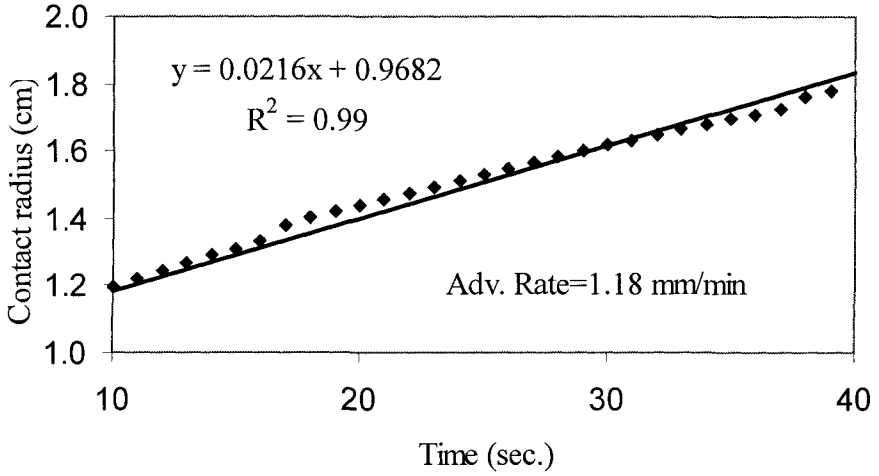

Figure 4.3 Advancing rate of the three-phase contact line calculated from the slope of the contact radius versus time

More than 20 different runs were conducted at various three-phase contact line speeds. The mean contact angle value for a specific advancing rate was obtained by averaging the measured contact angles over the span of the contact radius. The results show that the advancing contact angle was constant for three-phase contact-line advancing rates over almost 2 orders of magnitude (0.19-10.0 mm/min advancing rate) for both types of silicon wafers (type N and P), as shown in Fig. 4.4. By comparing the results of this study with the results of Kwok et al.[29], we see that this study extends the findings of Kwok et al. regarding independence of advancing contact angle from advancing rate by 1 order of magnitude for the system studied.

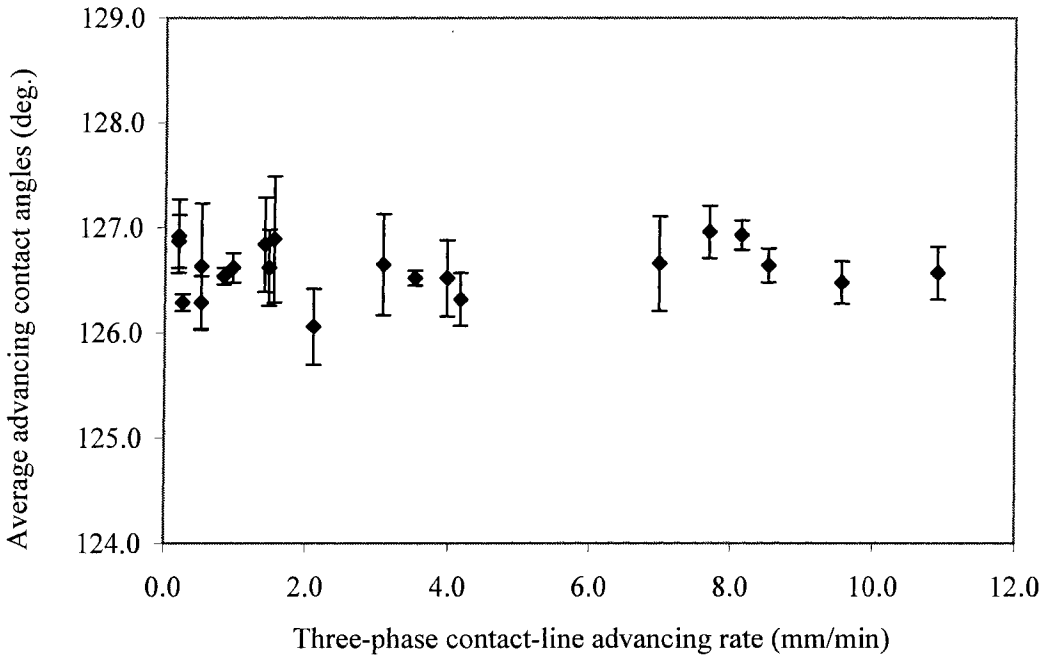

Figure. 4.4 Averages of advancing contact angles versus three-phase contact-line advancing rate in 1g. The error bars show the standard deviation from multiple runs at each rate.

As mentioned above, due to the short duration of the reduced gravity period, two different pumping rates were used in order to expand the drop to the maximum possible contact radius within one parabola and to keep the contact line advancing rate as constant as possible. The values of the advancing contact angle in reduced gravity are more variable than the ground results. It is believed that this variability could be due to the vibration in the airplane. The contact line advancing rate was determined in a similar way as explained in the previous section and was found to be about 7.96 mm/min (Fig. 4.5).

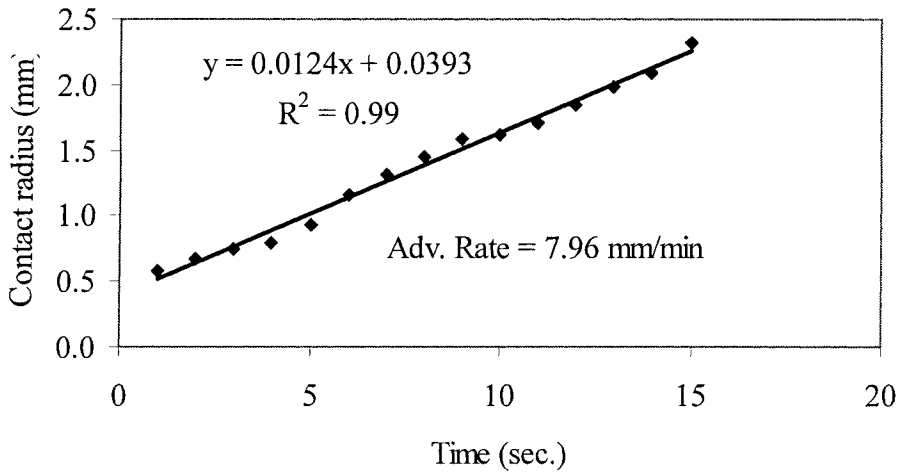

Figure 4.5 The advancing contact radius vs. time in ~0g

There is a clear difference of about 5° between the values of the advancing contact angle in reduced gravity and on ground, as can be seen in Fig. 4.6. This difference as discussed above could be due to changed hydrodynamics conditions within the drop. However, further investigation is required to delineate hydrodynamic effects from thermodynamic ones.

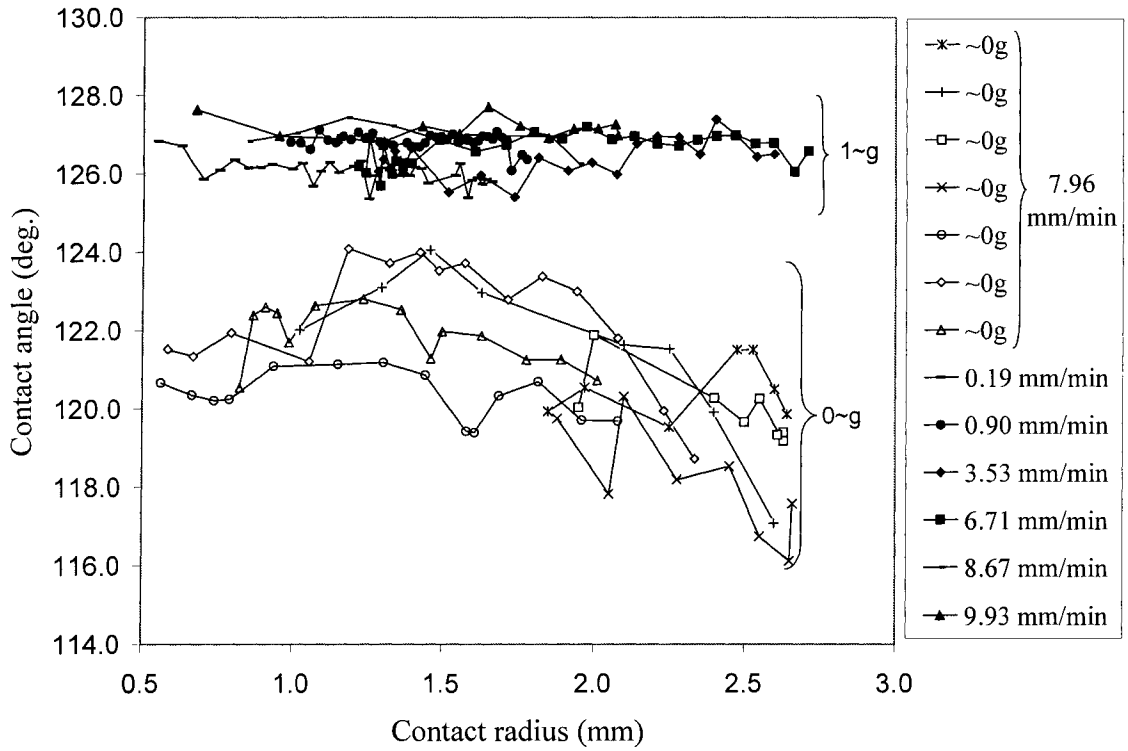

Figure 4.6 A comparison between the advancing contact angle for ground and reduced gravity environments

4.4. Conclusion

The effect of gravity on the advancing contact angle of a sessile drop has been determined experimentally by carrying out several reduced gravity and ground experiments. Even though the reduced gravity results were more variable than the ground results, there is a clear difference between the reduced gravity and the ground results. A difference of about 5° in the advancing contact angle was observed. These results will aid our understanding of the interaction of gravity and capillarity as they are the first measurements of sessile drop advancing contact angle showing a difference between near free fall and 1g.

CHAPTER 5

EFFECT OF ELECTROSTATIC FIELD ON SURFACE TENSION OF SESSILE DROPS

5.1. Introduction

The behavior of liquid drops and bubbles in electric fields is of fundamental importance in developing existing and new technologies on ground and in space, e.g., electrostatic spraying, ink jet printing, physical and chemical separation, and alloy research in space. One of the key properties in determining the behavior of drops is surface tension. The effect of electric field on surface tension of liquid drops is not understood well at the present time mainly due to the absence of a suitable methodology.

A new methodology was developed by another student (Arash Bateni) that can determine the possible effect of gravity and electric field on both shape and surface tension of drops. The new methodology, i.e., axisymmetric drop-shape analysis – electric fields (ADSA-EF), can generate numerical drop profiles as a function of surface tension, at any given gravity and/or electric field[31] . Where an image of an experimental drop is available, ADSA-EF can calculate a value of the surface tension by matching the numerical profiles with the shape of the experimental drop, taking the surface tension as an adjustable parameter. The objective of the experiment was to provide Arash Bateni with these images for analysis and verification of ADSA-EF. For detailed information about ADSA-EF, see reference [29].

5.2. Reduced Gravity Experiments

A series of experiments were conducted in a reduced gravity environment to study the effects of gravity and electric field on the shape and surface tension of drops using ADSA-EF. The reduced gravity environment was provided by Falcon 20 parabolic flights (provided by the National Research Council of Canada through an agreement with the Canadian Space Agency). The experiments were performed by forming drops of distilled water atop a Teflon-coated silicon wafer subject to variable potential ranging from 0 to 10 kV. The silicon wafer was placed on the top of the lower disk of a parallel plate capacitor with a distance of 8.8 mm between the plates. The volume of the drops was controlled by using a stepper motor and a controller. The base diameter of the drop was kept in the range of 2–3 mm. The drop was illuminated using a halogen lamp (Leica Model 13410311) in conjunction with diffuser glasses. Images of the drop were acquired using a CCD camera (Pixe-LINK) and saved on a computer before and after applying the electric field.

Figures 5.1 and 5.2 show the effect of the electric field on drop shapes (both images were acquired in reduced gravity). Fig. 5.1 shows a sessile drop of water in the absence of an electric field. Fig. 5.2 shows an image of a similar drop when an electric potential of 9 kV is applied. The drop is significantly-deformed by the electric field (elongated in the direction of the field). The images of the reduced gravity experiments were used as an input for ADSA-EF to calculate the surface tension of sessile drops in microgravity. There was no noticeable deformation of the hexadecane drops as can be seen in Fig. 5.3.

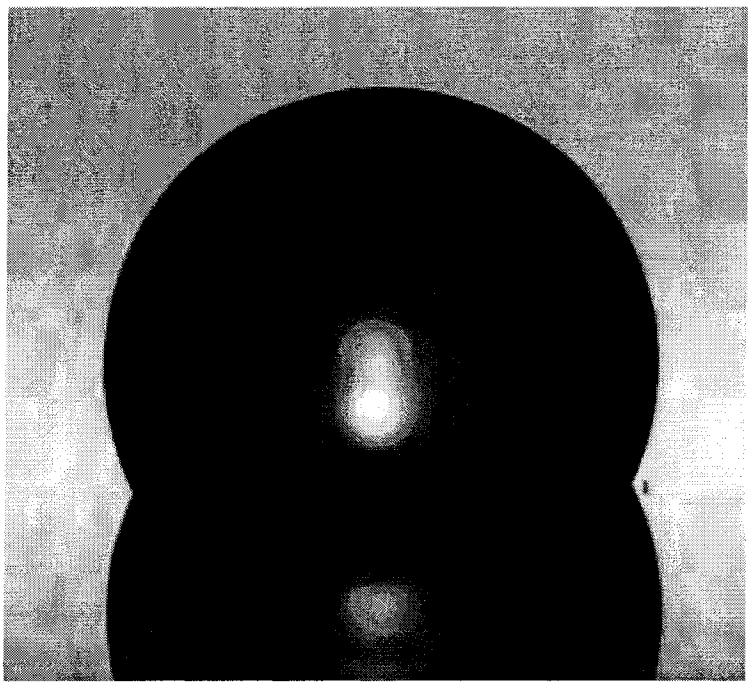

Figure 5.1. A 2 μℓ sessile drop of water on a Teflon-coated silicon wafer in reduced gravity when no electric field is applied

Figure 5.2 The same sessile drop of water as in figure 5.1 in reduced gravity conditions when an electric potential of 9 kV is applied. The drop is significantly deformed by the electric field

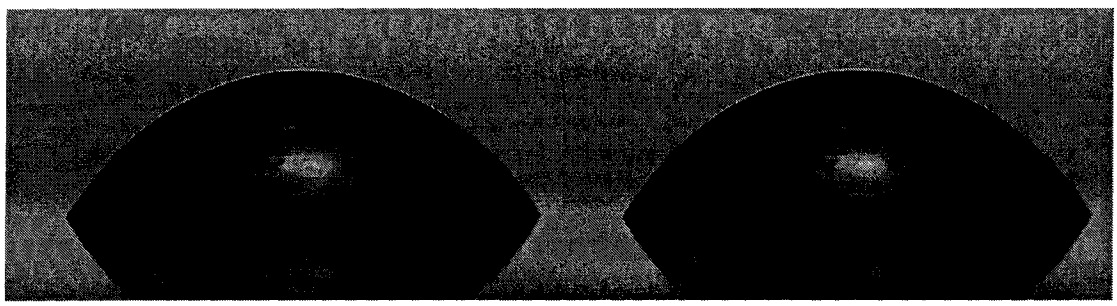

Figure 5.3 Hexadecane drop in microgravity: (left) no electric field, (right) with electric field

5.3. Results and Conclusion

Images of sessile drops under the effect of electrostatic field were acquired in microgravity. The images were sent to Arash Bateni at University of Toronto for analysis

and verification of ADSA-EF. Experimental work showed that the ADSA-EF-determined surface tension of water increases as a result of applied electric field. The results of ADSA-EF can be seen in Figure 5.3 as provided by Arash Bateni. As was expected, there is no effect of the electric field on the shape of the hexadecane drops due to the non-polarity of the hexadecane.

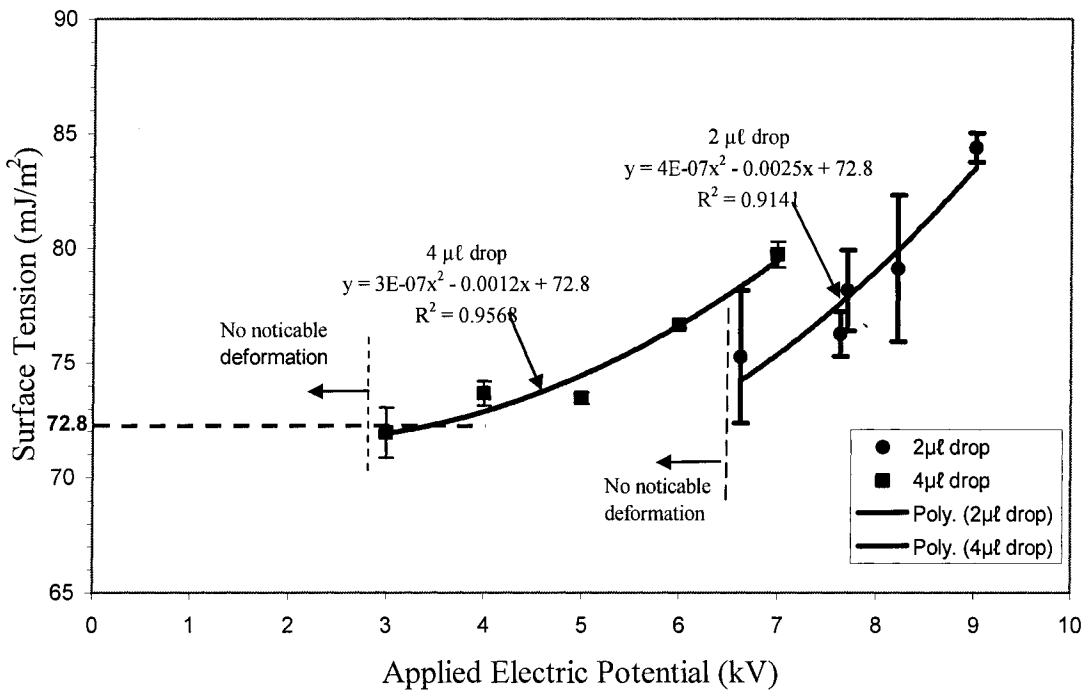

Figure 5.4 Calculated surface tension of water in reduced gravity in the presence of an electric field

CHAPTER 6

RECOMMENDATIONS AND CONCLUSIONS

The shape and surface tension of a droplet on horizontal surfaces have been studied experimentally for a long time. Still, several unsolved issues remain in this area. Most existing experimental works were focused on the effects of: the size of the droplet, the gas/liquid/solid materials, the surface roughness and, the heterogeneity of the solid surface. The present work which is the first study of its kind, is based on experimental data, obtained by performing experiments on the ground and aboard the Falcon 20 aircraft at the National Research Council, Flight Research Laboratory. The experimental setup makes possible the study of both "the effect of electrostatic field on the surface tension of sessile drops" and "the study of the effect of gravity on the advancing contact angle of sessile drops".

In this thesis, a difference of about 5° in the advancing contact angle was observed between the ground and microgravity environments. To investigate this difference, it is recommended to carry out a numerical study of the forced spreading of a drop with moving contact line. Flow fields containing moving contact lines also contain free surfaces. Since their location is not known *a priori*, they introduce additional difficulties into the associated boundary-value problem. Various techniques have been developed for dealing with this situation. Medjejski[32] employed an Overall Energy Balance (OEB) approach to model drop spreading, specifically considering the solidification of impinging drops on a cold surface. Medjeski proposed that the change in the total surface

and kinetic energy of the drop is completely balanced by internal viscous losses. Gu and Li used the same approach to model both spontaneous[33] and low speed impact[34] drop spreading. Then, Erickson, Blackmore and Li[35] extended this approach to study forced spreading where the primary driving force is hydrodynamic in nature. In forced spreading, the spreading is accomplished through the addition of liquid (mass) to the system. In the analysis, the authors assumed that the dynamic contact angle is known *a priori* from the measurements and they were looking for the contact line advancing rate. The authors also included the effect of gravity as a separate term in the OEB equation but they assumed a spherical cap shape of the drop. Figure 6.1 shows a schematic of a growing droplet on a smooth, rigid and homogeneous solid surface. The primary driving force behind drop spreading in this case is the quasi-steady addition of the liquid to the system through a hole in the surface (at point O).

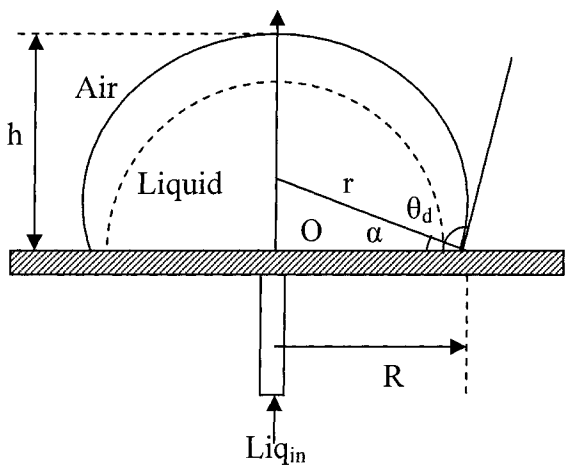

Figure 6.1 Schematic diagram of hydrodynamically forced spreading of a sessile drop on a solid surface

The general overall energy balance for the system shown in figure 6.1 is given by:

$$\frac{dE_{in}}{dt} = \frac{d}{dt}(E_{sys} + E_s + E_g + Q) + \frac{d}{dt}(W_v + W_b) \tag{6.1}$$

where the energy entering the system (E_{in}) is balanced with the change in internal energy of the system (E_{sys}), increase or decrease in surface energy (E_s), gravitational potential energy (E_g), heat transfer (Q), boundary movement work (W_b), and the viscous dissipation work (W_v).

Experimental work was performed to investigate the effect of external forces, i.e., gravity and electric field, on shape and surface tension of drops. A new methodology, introduced by Arash Batani, called axisymmetric drop-shape analysis – electric fields (ADSA-EF), can generate numerical drop profiles as a function of surface tension, at any given gravity and/or electric field. When an image of an experimental drop is available, ADSA-EF can calculate the true value of the surface tension by matching the numerical profiles with the shape of the experimental drop, taking the surface tension as an adjustable parameter. The mechanical equilibrium between the surface tension, the electric field and gravity can be described mathematically by the augmented Young–Laplace equation[31]

$$\gamma\left(\frac{1}{R_1} + \frac{1}{R_2}\right) = \Delta P_o + (\Delta\rho)gz + \Delta P_e \tag{6.2}$$

Where γ is the surface tension, R_1 and R_2 are the two principal radii of curvature, ΔP_0 is the pressure difference across the interface at the reference (i.e., the apex of the drop), $\Delta\rho$ is the density difference across the interface, g is the gravitational acceleration, z is the vertical distance of any point on the drop surface from the reference, and ΔP_e is the electrical pressure (i.e., the jump in the normal component of the Maxwell stress tensor across the interface). Due to the symmetrical nature of the problem, ADSA-EF calculates the surface tension at the apex of the drop where the radius of curvature is constant in all directions. Experimental work showed that the ADSA-EF-determined surface tension of water increases as a result of applied electric field. Qualitative extrapolation of results suggested the same surface tension at zero electric field that was obtained on the ground. That is, no significant effect of gravity on surface tension was observed.

REFERENCES

[1] Encyclopedia Britannica, Inc., Vol. 21, (593-602), 1947.

[2] Young T., "Essay on the Cohesion of Fluids", Roy. Phill. Transections (65-87), December 20, 1805.

[3] Laplace P. S.,"Celestial mechanics. Translated with a commentary, by Nathaniel Bowditch" Bronx, N. Y., Chelsea (1966).

[4] Encyclopedia Britannica, Inc., Vol. 21, (593-694), 1929.

[5] Rayleigh, "Scientific Papers", Vol. VI, New York, Dover Publications (1964).

[6] Gibbs J. W., "The Collected Works of J. Willard Gibbs", Vol. 2, Longmans, Green. and co., 1928.

[7] Langmuir I., "The Constitution and Fundamental Properties of Solids and Liquids", J. Am. Chem. Soc., Vol. 38(11), 2221-2295 (1916).

[8] Harkins W. D.,"The physical chemistry of surface films; with a foreword by Peter Debye", New York, Reinhold, 1952.

[9] Adam N. K., "The Physics and Chemistry of Surfaces", Oxford university press, H. Milford, 1941.

[10] Burdon R. S., "Surface Tension and the Spreading of Liquids", Cambridge University Press, London, 1949.

[11] Purohit G. P., "Experimental Investigations of Stability of Static Liquid Fillets and Liquid-Gas Interface in Capillary Passages for Gas-Free Acquisition in Zero Gravity", Ph.D. Thesis, UCLA, 1998.

[12] Adamson A. W., "Physical Chemistry of Surfaces". 4th ed., John Wiley and Sons, (1982).

[13] Neumann A. W., "Applied Surface Thermodynamics, Surfactant Science Series", Vol. 63, Marcel Dekker, Inc. (1996).

[14] Du Noûy P. L., "A New Apparatus for Measuring Surface Tension", J. Gen. Physiol., 1, 521 (1919).

[15] Wilhelmy L., Ann. Phys., 119, 177(1863).

[16] Rotenberg Y. Boruvka L. and Neumann A. W., J Colloid Interface Sci., 130, 25(1989).

[17] http://www.space.gc.ca/asc/pdf/FalconUserGuide2001.pdf. Nov., 24/2005.

[18]Bateni A., Ababneh A. , Elliott J.A.W., Neumann A.W., Amirfazli A., "Effect of gravity and electricfield on shape and surface tension of drops", Adv. Research in Space, accepted 26 February 2005.

[19] Dussan V. E. B., "On the spreading of liquids on solid surfaces: static and dynamic contact lines", Ann. Rev. Fluid Mech. 11, 371-400 (1979).

[20] Kowk D. Y. , Lam C. N. C., Leung A., Mok R. Wu, E. , Neumann A. W., "Measuring and interpreting contact angles: a complex issue", Colloid. Surfaces, A. 142, 219-235 (1998).

[21] Wege H. A. , Aguilar J. A. , Rodriguez-Vaverde M. A., Toledano M., Osorio R. , Cabrerizo-Vilchez M. A., "Dynamic contact angle and spreading rate measurements for the characterization of the effect of dentin surface treatment", J. Colloid Interface Sci. 263, 162-169 (2003).

[22] Ngan C. G., Dussan V. E. B., "On the dynamics of fluid spreading on solid surfaces", J. Fluid Mech. 209, 191-226 (1989).

[23] Blake T. D., Bracke M., and Shikhmurzaev Y. D, "Experimental evidence of nonlocal hydrodynamic influence on the dynamic contact angle", Phys. Fluids 11, 1995-2007 (1999).

[24] Ward C. A., Rahimi P., Sasges M. R., and Stanga D., "Contact angle hysteresis generated by the residual gravitational field of the space shuttle", J. Chem. Phys., 112(16), 7195-7202 (2000).

[25] Sasges M. R. and Ward C. A., "Effect of gravity on contact angle: An experimental investigation", J. Chem. Phys., 109(9), 3661-3670 (1998).

[26] Ward C. A. and Sasges M. R., "Effect of gravity on contact angle: A theoretical investigation", J. Chem. Phys., 109(9), 3651-3660 (1998).

[27] Abel G., Ross G. G. and Andrzejewski L., "Wetting of a liquid surface by another immiscible liquid in microgravity", Adv. Space Res. 33, 1431-1438 (2004).

[28] Dreyer M., Delagado A. and Rath H.-J., "Capillary rise of a liquid between parallel plates under microgravity", J. Colloid. Interface. Sci. 163, 158-168 (1994).

[29] Kowk D.Y., Lin R., Mui M., Neumann A.W., "Low-rate dynamic and static contact angles and the determination of solid surface tensions", Colloid Surfaces A, 116, 63-77 (1996).

[30] Blake T. D. and Shikhmurzaev Y. D., "Dynamic wetting by liquids of different viscosity", J. Colloid Interface Sci. 253 196-202 (2002).

[31] Bateni A., Susnar S.S., Amirfazli A., Neumann A.W. "Development of a new methodology to study drop shape and surface tension in electric fields". Langmuir 20, 7589–7597 (2004).

[32] Madejski J., "Solidification of droplets on a cold surface", Int. J. Heat Mass Trans., 19, 1009-1013 (1976).

[33] Gu Y., Li D., "A model for a liquid drop spreading on a solid surface", Coll. Surf. A, 142, 243-259 (1998).

[34] Gu Y., Li D., "Liquid drop spreading on solid surfaces at low impact speeds", Coll. Surf. A, 163, 239-245 (2000).

[35] Erickson D., Blackmore B., Li D., "An energy balance approach to modeling the hydrodynamically driven spreading of a liquid drop", Coll. Surf. A, 182, 109-122 (2001).

APPENDIX-A

Test Cell Drawings

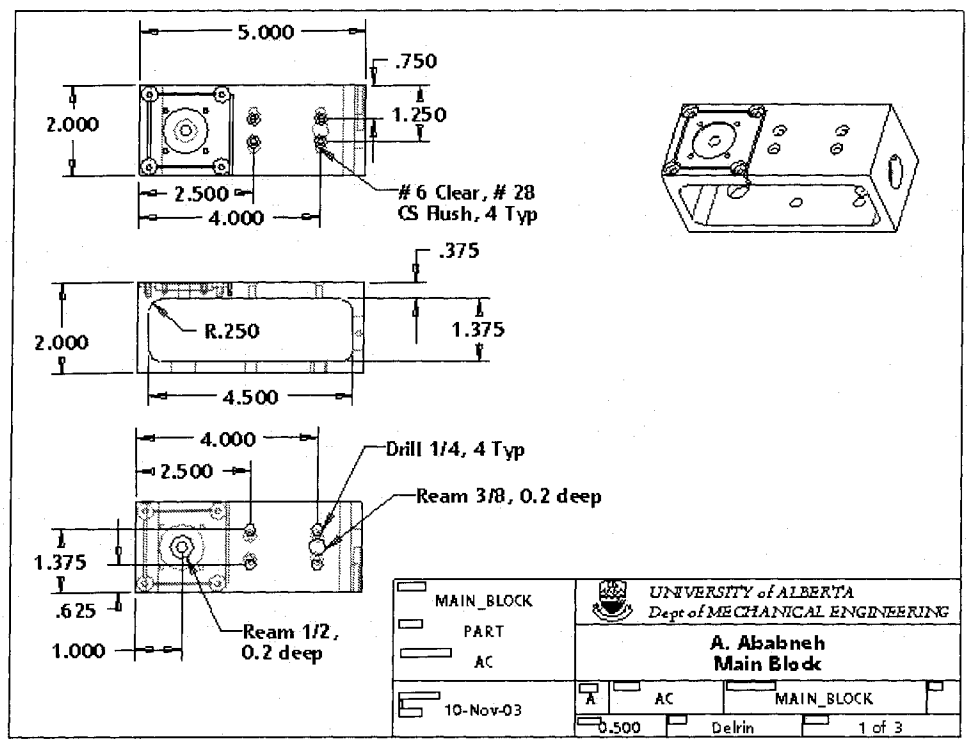

Figure A-1. Main block

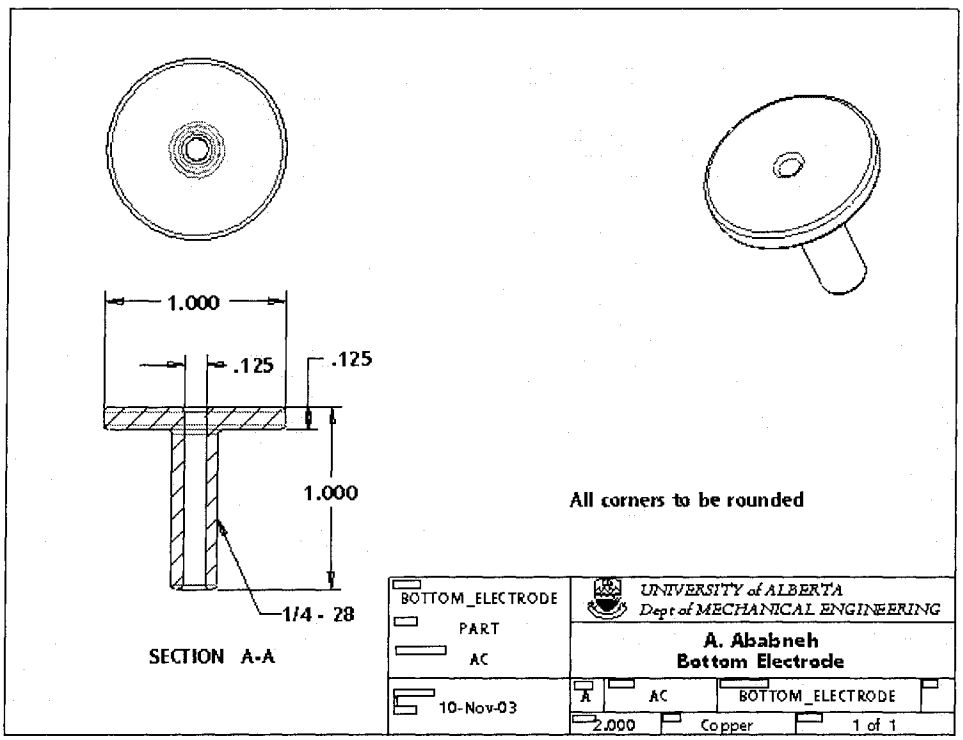

Figure A-2. Bottom electrode

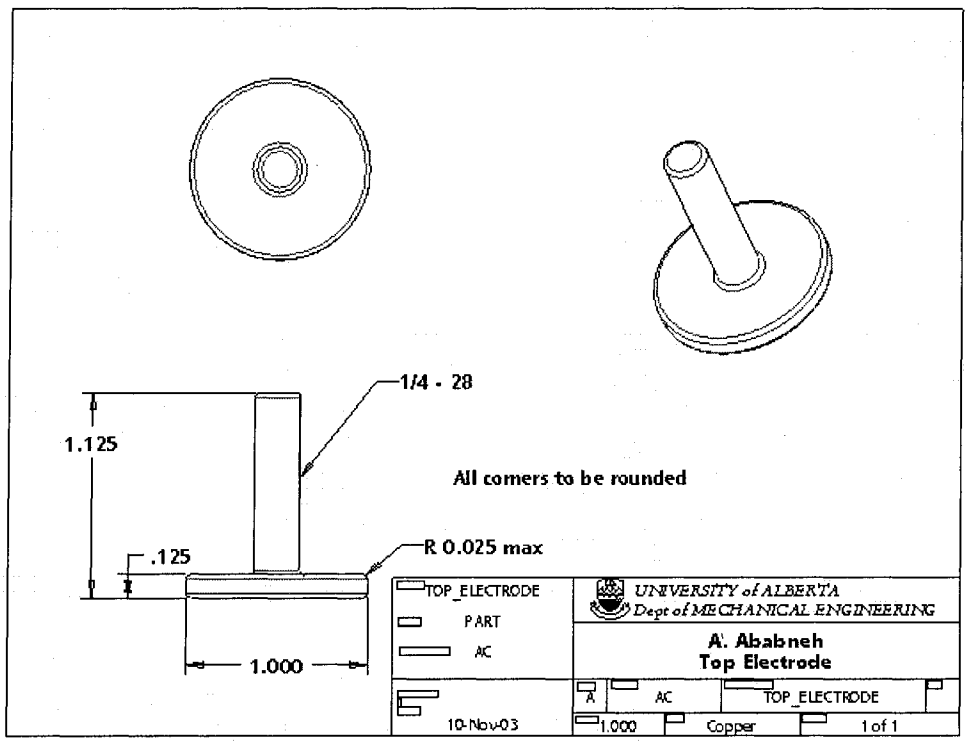

Figure A-3. Top electrode

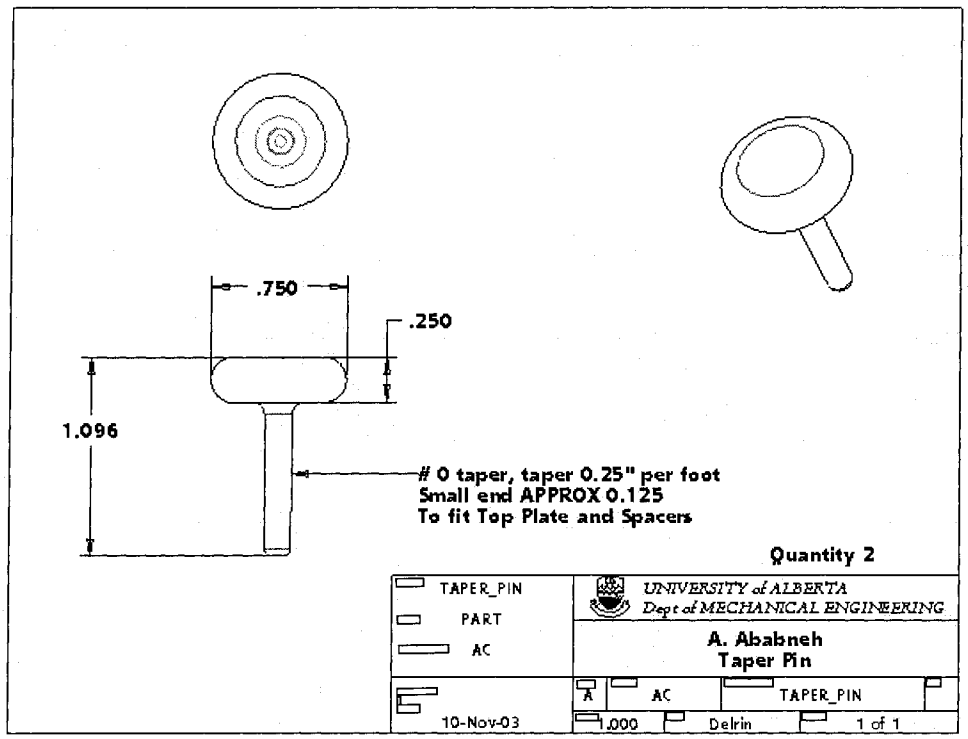

Figure A-4. Taper pin

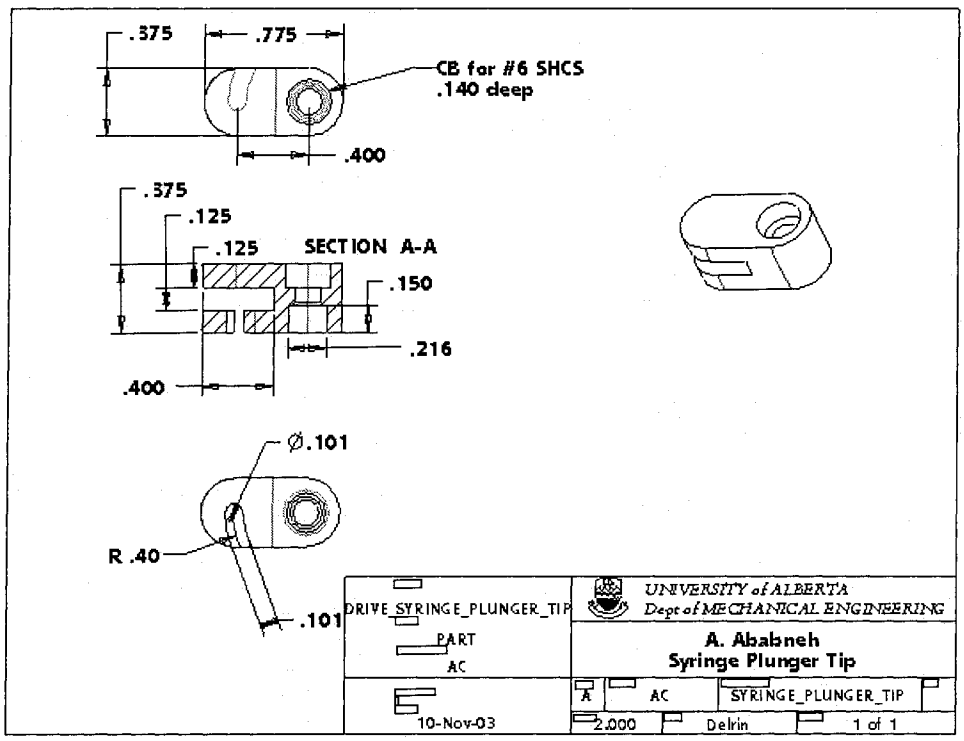

Figure A-5. Syringe plunger tip

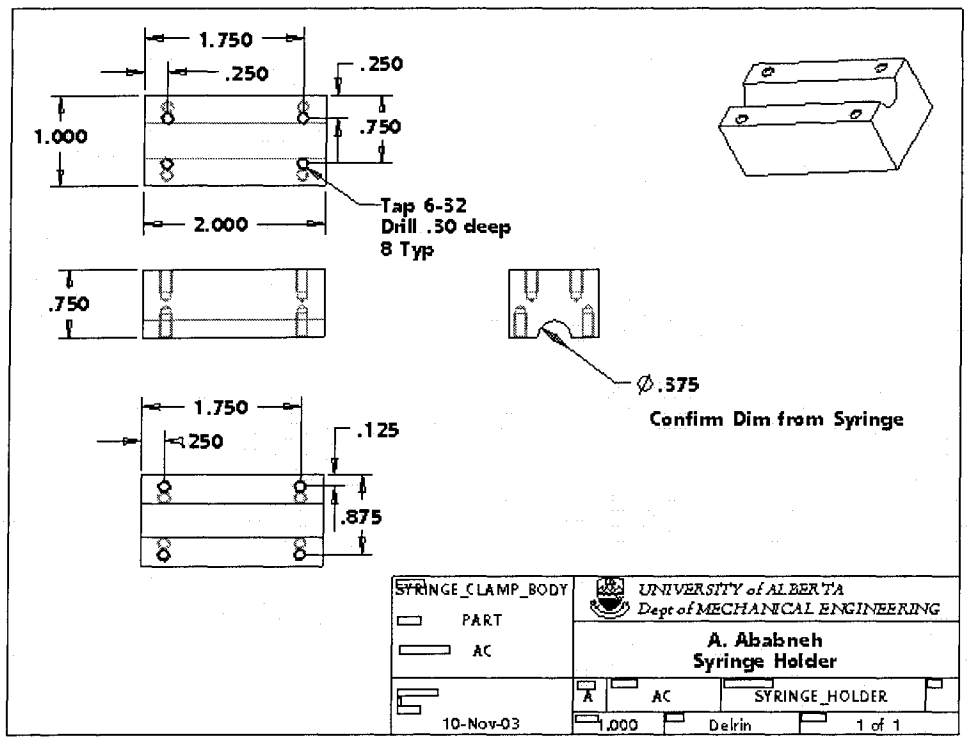

Figure A-6. Syringe holder

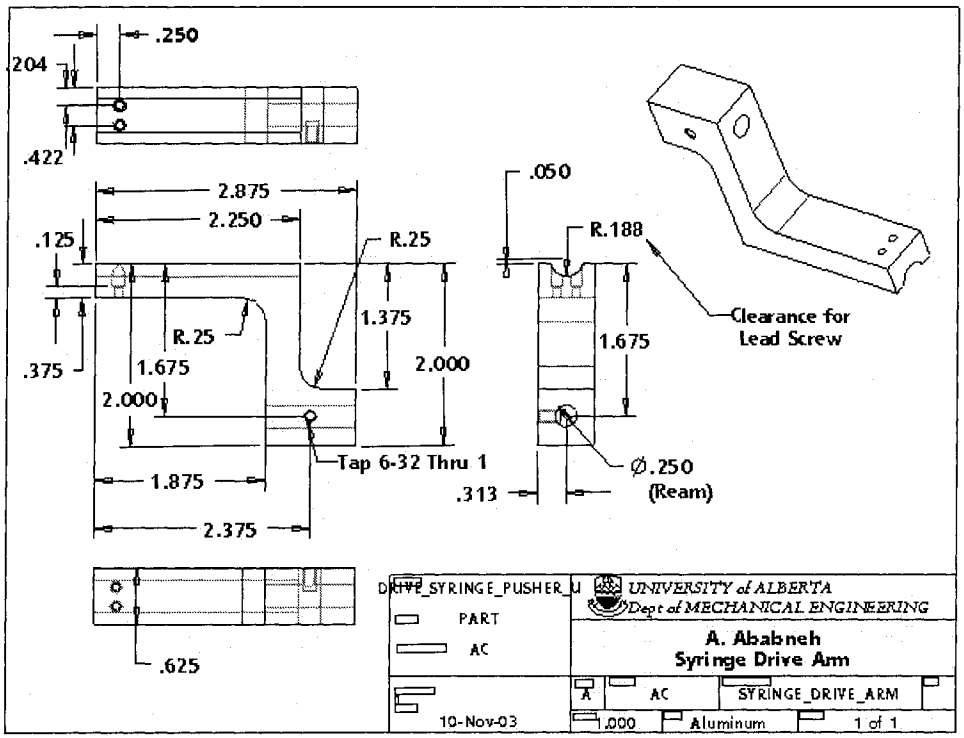

Figure A-7. Syringe drive arm

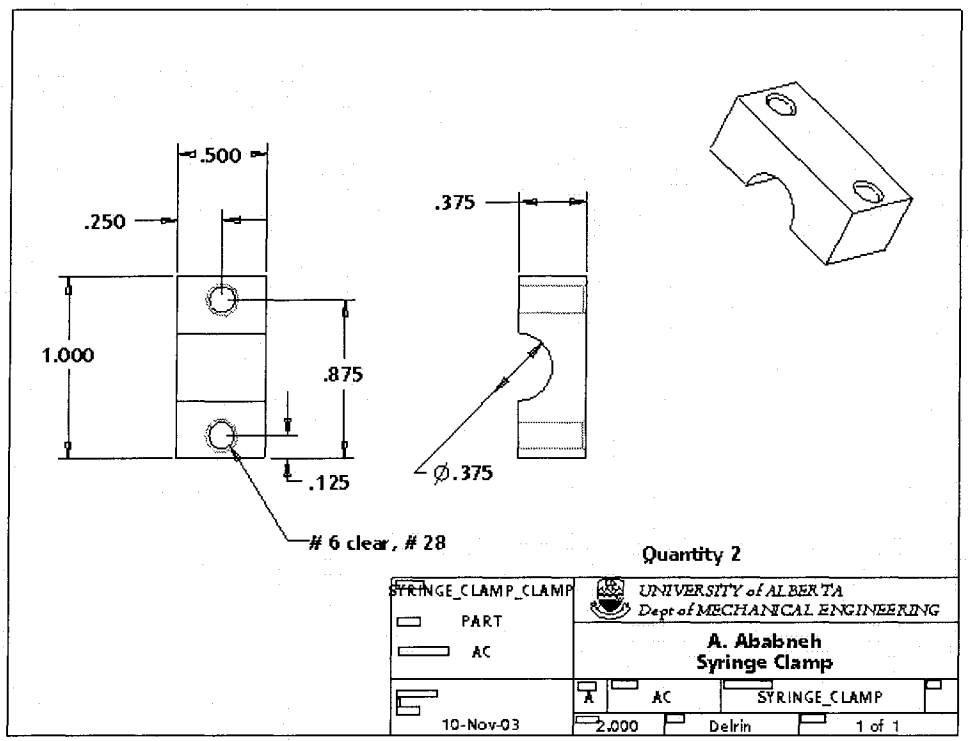

Figure A-8. Syringe clamp

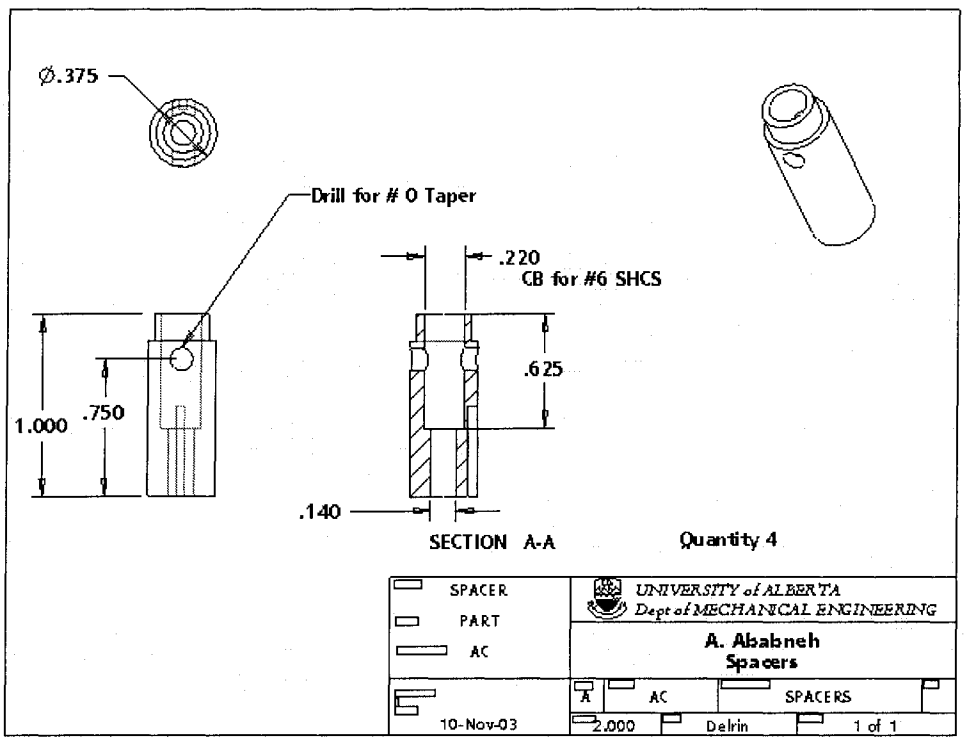

Figure A-9. Spacer

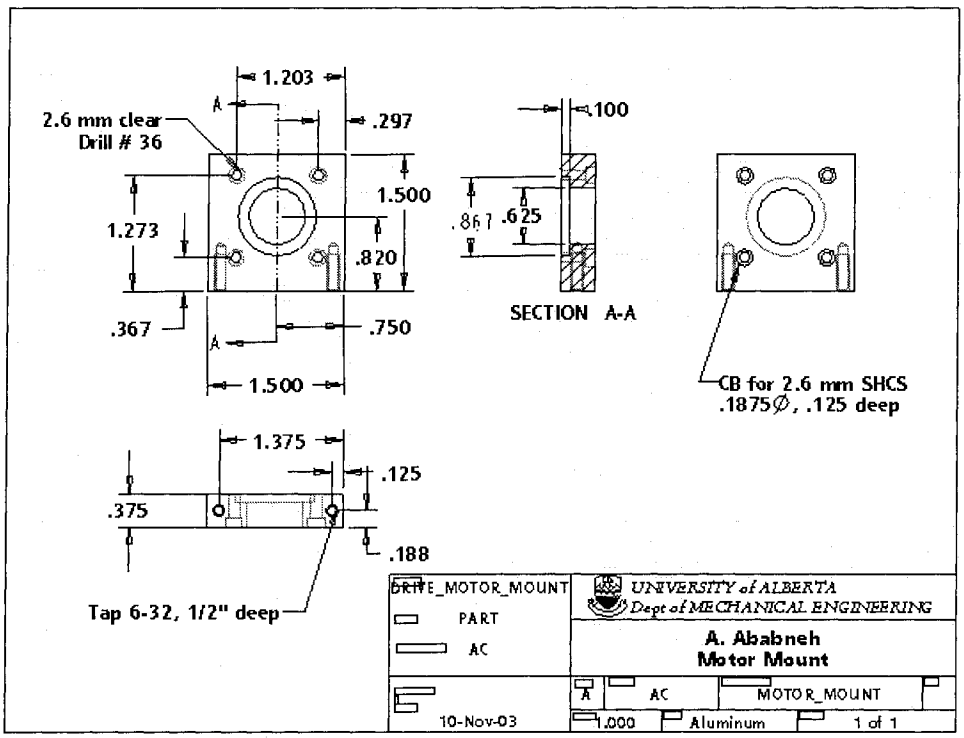

Figure A-10. Motor mount

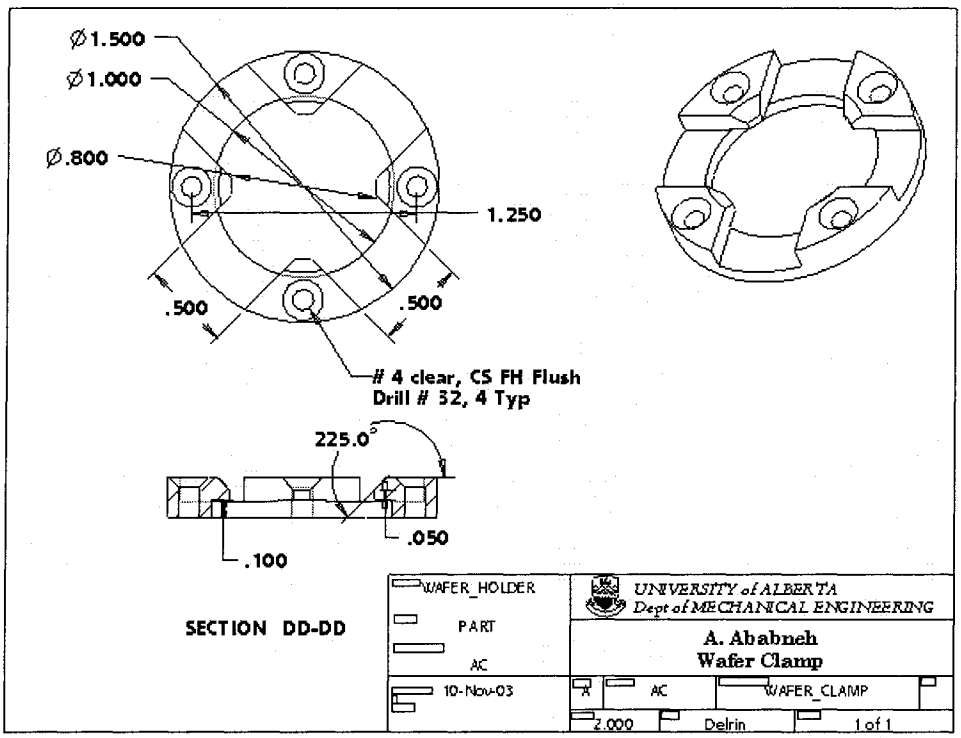

Figure A-11. Wafer clamp

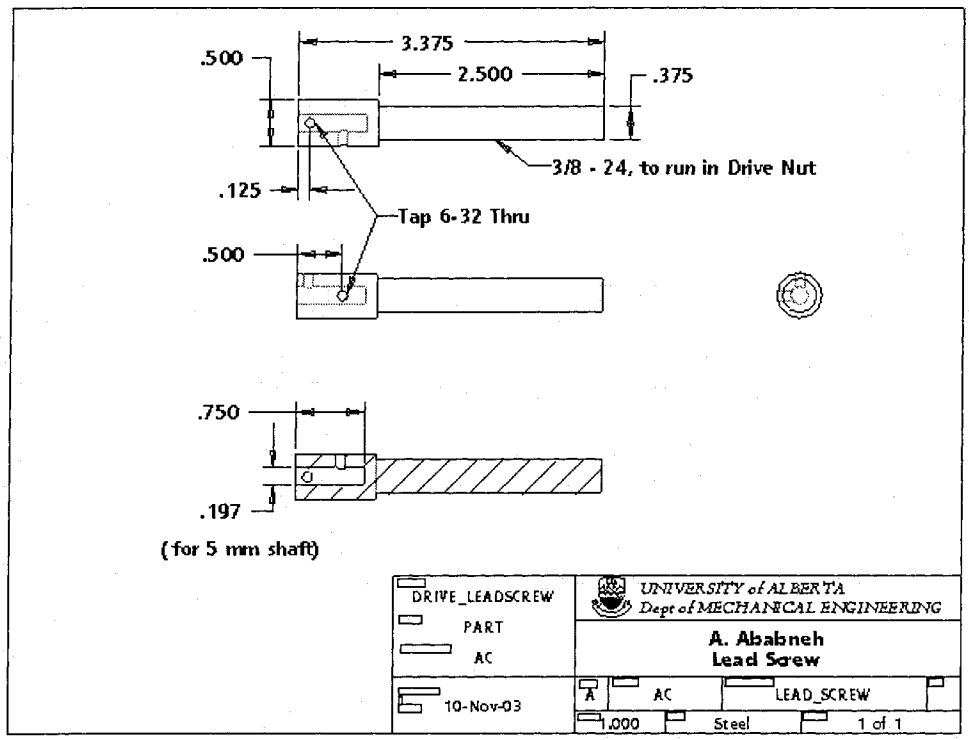

Figure A-12. Lead screw

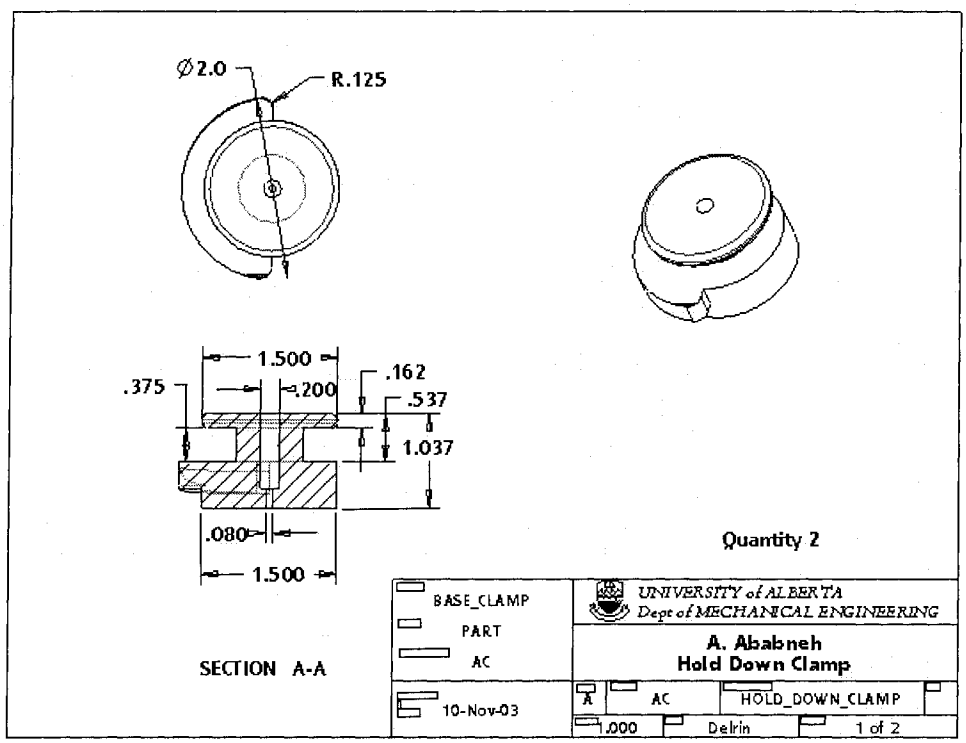

Figure A-13. Hold-down clamp

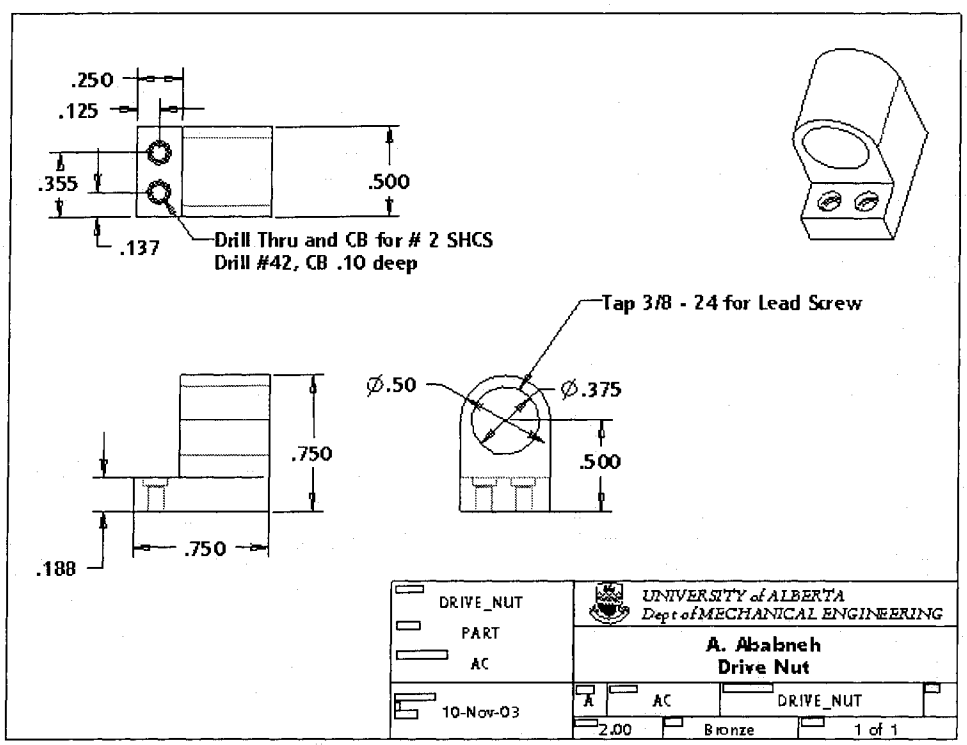

Figure A-14. Drive nut

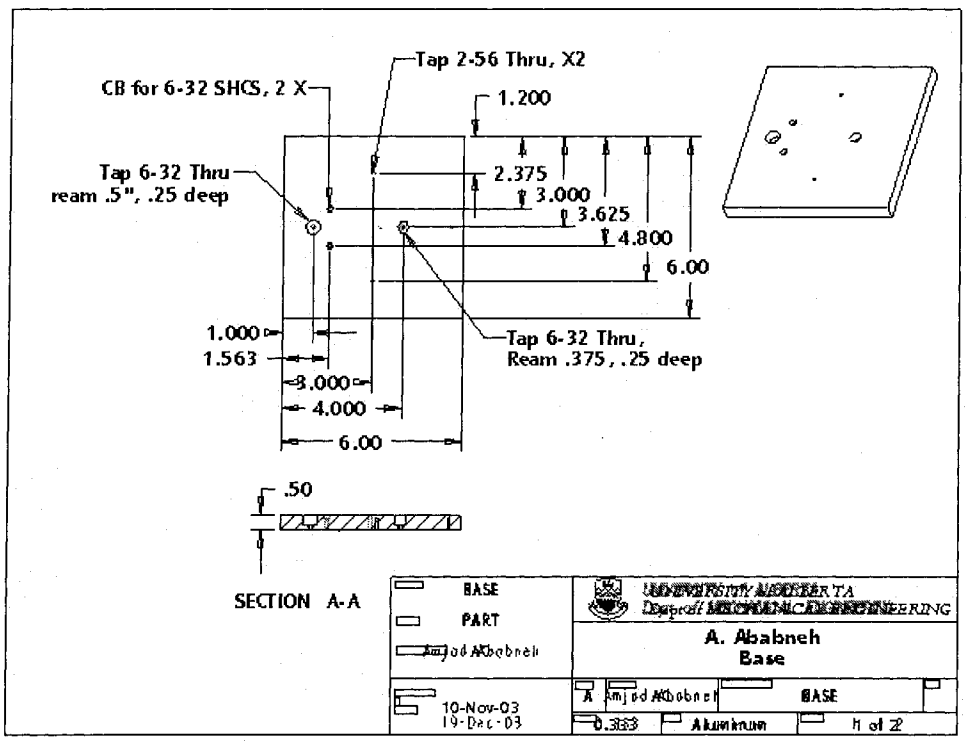

Figure A-15. Base plate

APPENDIX-B

Checklist of checkpoints for microgravity experiments

1. All nuts and pins are tightened and secured.
2. No floating wires or objects (all wires are strapped or taped down).
3. The test cells are available and secured.
4. All electric wires are securely connected.
5. The syringes in each cell are filled with the desired liquid for each parabola.
6. No air bubbles in the syringes.
7. One of the test cells is clamped down tight to the test cell plate.
8. All electric terminals are plugged in to the power bar and the power bar is plugged in to the onboard power source.
9. Camcorder battery is full.
10. New and clean tape in camcorder.
11. Backlight is working properly by turning the light on and changing the light intensity.
12. Laptop is working properly, power options settings are not on standby or hibernating mode.
13. Programs needed, i.e. the frame grabber and the stepper motor drive (Si Programmer™ software) are installed and working properly.
14. The CCD camera and camcorder are in focus.

For the electric field experiments, the following additional points were checked:

1. The high voltage power supply connected to the electric field disks through the high voltage power connectors.

2. The variable voltage of the main power supply is set to zero while the current is set to maximum.

3. 25μℓ syringes are filled with the desired liquid (water or hexadecane).